

KNOT TIGHTENING BY CONSTRAINED GRADIENT DESCENT

TED ASHTON, JASON CANTARELLA, MICHAEL PIATEK, AND ERIC RAWDON

ABSTRACT. We present new computations of approximately length-minimizing polygons with fixed thickness. These curves model the centerlines of “tight” knotted tubes with minimal length and fixed circular cross-section. Our curves approximately minimize the ropelength (or quotient of length and thickness) for polygons in their knot types. While previous authors have minimized ropelength for polygons using simulated annealing, the new idea in our code is to minimize length over the set of polygons of thickness at least one using a version of constrained gradient descent.

We rewrite the problem in terms of minimizing the length of the polygon subject to an infinite family of differentiable constraint functions. We prove that the polyhedral cone of variations of a polygon of thickness one which do not decrease thickness to first order is finitely generated, and give an explicit set of generators. Using this cone we give a first-order minimization procedure and a Karush-Kuhn-Tucker criterion for polygonal ropelength criticality.

Our main numerical contribution is a set of 379 almost-critical knots and links, including all prime knots with ten and fewer crossings and all prime links with nine and fewer crossings. For links, these are the first published ropelength figures, and for knots they improve on existing figures. We give new maps of the self-contacts of these knots and links, and discover some highly symmetric tight knots with particularly simple looking self-contact maps.

1. INTRODUCTION

Overview. Knots tied in rope are flexible machines which organize tensions and contact forces to bind tightly and resist unravelling. As a technology, knots have proved remarkably effective. For this reason there is a vast body of knowledge about their practical uses. Yet in many ways, the design of these machines remains mysterious. As early as 1987 Maddocks and Keller were able to study different types of hitches and predict their holding power by an analysis of their equilibrium shapes [34]. But these shapes were rather simple, and there was no way to infer the structures of more complicated knots from these examples. It was obvious that what was needed was data, and by the end of the century a series of numerical experiments in knot-tightening were underway [44, 41, 32, 52]. This paper describes a new computational approach to knot-tightening which yields improved numerical results (a preliminary report on some of our findings appeared in the conference proceedings [13]). To build our method, we derive some new results in the theory of ropelength for polygonal knots.

Date: June 12, 2004; Revised: November 18, 2018.

Key words and phrases. ropelength, tight knots, ideal knots, constrained gradient descent, sparse non-negative least squares problem (snls), knot-tightening.

Defining the problem. Given any space curve γ , we can define the *thickness* $\text{Thi}(\gamma)$ of γ to be the supremal ϵ for which any point in an ϵ -neighborhood of γ has a unique nearest neighbor on the curve¹. Any curve with nonzero thickness is $C^{1,1}$ (that is, is C^1 with a Lipschitz first derivative) [22, 11]. Given this, it has been shown that

Proposition 1.1 ([33]). *If γ is a C^1 curve, then the thickness $\text{Thi}(\gamma)$ is given by the supremal radius of all embedded tubes formed by taking the union of disks of uniform radius centered on $\gamma(s)$ in the planes normal to $\gamma'(s)$.*

This idea of thickness was first proposed by Krötenheerdt and Veit in 1976 [30, 31] and was rediscovered in the 1990's by Nabutovsky [37] and Buck and Orloff [6]. The thickness can be used to define a scale-invariant quantity called *ropelength*:

Definition 1.2. The *ropelength* of a curve γ is defined by

$$\text{Rop}(\gamma) = \frac{\text{Len}(\gamma)}{\text{Thi}(\gamma)},$$

where $\text{Len}(\gamma)$ is the length of γ . The *minimal ropelength* of a knot or link type L , $\text{Rop}(L)$, is the minimal ropelength of all curves in that knot or link type.

The knot tightening problem is to find and describe the minimal ropelength curves in a given knot type. It is known that such curves exist, but their exact shapes are currently the subject of active mathematical research (c.f. [25, 26, 11]). Once found (or computed to sufficient accuracy), these configurations have been used to predict the relative speed of DNA knots under gel electrophoresis [28], the pitch of double helical DNA [36], the average values of different spatial measurements of random knots [20], and the breaking points of knots [42]. They also provide a model for the structure of a class of subatomic particles known as glueballs [8].

Another form of the problem. Let $\gamma: S^1 \rightarrow \mathbb{R}^3$ now be a C^2 parametrized curve, and define the self-distance function $d: S^1 \times S^1 \rightarrow \mathbb{R}$ of γ by $d(s, t) := \|\gamma(s) - \gamma(t)\|$. As usual, let $\kappa(s)$ denote the curvature of γ . We then define the set $\text{dcsd}(\gamma)$ of *doubly-critical self-distances* to be the set of critical points of d with $s \neq t$. Taking the partial derivatives of d , we see that $(s, t) \in \text{dcsd}(\gamma)$ if and only if

$$\langle \gamma(s) - \gamma(t), \gamma'(s) \rangle = 0 \text{ and } \langle \gamma(s) - \gamma(t), \gamma'(t) \rangle = 0.$$

A key idea in [33] is that for any $\tau < \text{Thi}(\gamma)$, the surface of the tube of radius τ around γ has no self-intersections and is C^2 smooth. But when $\tau = \text{Thi}(\gamma)$, the tube is pinched or has a tangential self-intersection. This leads to an alternate characterization of thickness:

Theorem 1.3 ([33]). *The thickness of γ is the minimum of*

$$\min_s \frac{1}{\kappa(s)} \text{ and } \min_{(s,t) \in \text{dcsd}(\gamma)} \frac{d(s,t)}{2}.$$

Figure 1 shows curves where the first and second of these terms control the thickness.

¹Federer referred to this number as the *reach* of γ [22].

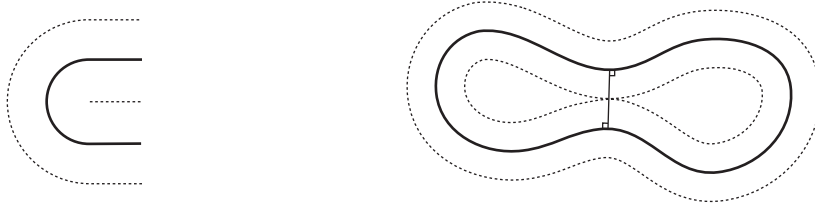


FIGURE 1. The thickness of a smooth curve γ is controlled by curvature (as in the left picture), and the length of chords in $\text{dcsd}(\gamma)$ (as in the right picture).

Since length and thickness scale together, minimizing ropelength is the same as minimizing length over the set of curves with thickness at least one. Since thickness is a min-function, the condition $\text{Thi}(\gamma) \geq 1$ can be viewed as an infinite family of inequality constraints on γ . These constraints are active at places where the tube around γ forms kinks (where $1/\kappa$ is in control of the minimum in Theorem 1.3) or has self-contacts (where the self-distance $d^{(s,t)}/2$ is in control of the minimum).

Numerical approaches to the knot-tightening problem. Previous authors have defined discretized versions of thickness for polygons or spline curves and viewed the problem as one of minimizing the nonsmooth quotient of length and thickness. The advantage of this approach is that it is a very simple and robust way to obtain approximately ropelength-minimizing curves. The disadvantage is that it is very difficult to take advantage of the fact that thickness (as given in Thm 1.3) is a min-function.

Our approach is to define a discrete version of thickness as a min-function and think of the problem as one of minimizing a differentiable function $\text{Len}(\mathcal{V})$ subject to a family of differentiable constraints $\text{Thi}_p(\mathcal{V}) \geq 1$. While our approach will not quite fit into the standard framework of constrained optimization (our family of constraints is infinite), we will be able to define a version of constrained gradient descent which minimizes polygonal ropelength effectively.

Theoretical framework. For an equilateral space polygon \mathcal{V} we first prove that our function $\text{Thi}_p(\mathcal{V})$ can be written as a min over a fixed compact family of differential functions. From here we use Clark's theorem to show that Thi_p has a one-sided derivative in the direction of any variation W of \mathcal{V} . For a polygon with $\text{Thi}_p(\mathcal{V}) = 1$ we use these derivatives to define a cone of infinitesimal variations $I(\mathcal{V})$ which do not decrease Thi_p to first order and the dual cone of "resolvable" variations $R(\mathcal{V})$. Our next main theorem is that $R(\mathcal{V})$ is a finitely generated polyhedral cone whose generators are the gradients of the lengths of certain chords of the polygon (called *struts*) and of a function of certain turning angles of the polygon (called *kinks*). We give explicit formulae for these gradients in terms of the vertex positions. We then compute the gradient of $\text{Len}(\mathcal{V})$ and define the constrained gradient of length to be the projection of $\text{Len}(\mathcal{V})$ onto the polyhedral cone $I(\mathcal{V})$. At this point we give the expected result that a polygon is critical for polygonal ropelength if and only if the constrained gradient of length is zero. Equivalently, a polygon is critical for polygonal ropelength if there is a set of positive Lagrange multipliers on the struts and kinks which combine to equal the negative of the length gradient. The theory section ends with a discussion of how to compute the constrained gradient numerically.

Numerical methods. Sections 3 and 4 describe the design of our polygonal ropelength minimizing software. Our algorithm essentially consists of computing the constrained gradient of length and taking small steps in this direction until the constrained gradient is sufficiently small. However, the details of the process are not quite so simple. Since the constraint functions are nonlinear, even steps that are in the direction of the constrained gradient violate some constraints to second order. Further, newly active constraints are discovered throughout the run as previously distant sections of tube come into contact with one another. As a result, we must choose stepsizes carefully and correct errors periodically. It is also important to run efficiently, as the size of our problem (about one thousand variables and a similar number of active constraints) is fairly large. We have solved these technical and engineering problems and used our software to minimize all prime knots with ten or fewer crossings and all prime links with nine or fewer crossings, for a total of 379 different knot and link types. We intend to address the ropelength of composite knots and links in a future publication.

New ropelength bounds. We check our figures against previous computations of the minimum ropelength of knots and links and against some of the few known theoretical results for the lengths of tight links. Our results improve on all previously published computational results except for the trefoil knot. For example, we improve the best known upper bound for the ropelength of the well-studied figure-eight knot 4_1 by 0.06 to 42.0887 (as compared to the bound of [14]) and improve the best known upper bound for the ropelength of the 9_{20} knot by 8.12% to 80.2219 (compared to the bound of [47]). To get a sense of the difference between the configurations produced by our method and the configurations produced by the simulated annealer of [47] we show both configurations in Figure 2. For links, our figures are the first computational results to appear in print, but compare well to known theoretical results. For example, the upper bound provided by our computation of the Borromean rings link 6_2^3 is 58.0070 — within 0.0017% of the exact value around 58.0060 suggested by [10], while our computation of the tight shape of the “simple chain” link is 41.7086588 — within 0.02% of the correct value of $6\pi + 2$ [11].

We also compared our results to those of Gilbert [24], which are unpublished but available on Bar-Natan’s *Knot Atlas* wiki. Gilbert provides Fourier coefficients and instructions for reconstructing the vertices of his configurations from this data. We followed his instructions, but our software did not verify his claimed ropelength numbers². According to our measurement of the ropelength of Gilbert’s configurations, our knots are tighter in all cases but 2_1^2 by an average of 3.619%, with some outliers, such as our 9_{37}^2 link, which is 71% shorter. If we compare our results to Gilbert’s claimed ropelengths, our knots and links are tighter in 316 cases and less tight in 36. Overall, our knots and links are (on average) 1.075% tighter than the bounds claimed by Gilbert with our 9_{28}^2 link about 4% shorter than Gilbert’s claim.

Self-contact maps. Two sets of authors (von der Mosel et al. [50] and Cantarella et al. [10]) have given versions of a ropelength criticality criterion for knots without kinks which state roughly that a knot γ is ropelength-critical when the elastic force given by the gradient of the length of the curve is balanced by a system of Lagrange multipliers on the self-contacts of the tube around γ . The latter

²Our measurement of curvature by MinRad is sensitive to edglength and seems to come out much larger than his ropelengths would indicate. This is probably a discretization effect, and it is certainly very possible that the Fourier knots defined by Gilbert’s data have ropelengths corresponding to Gilbert’s claimed numbers.

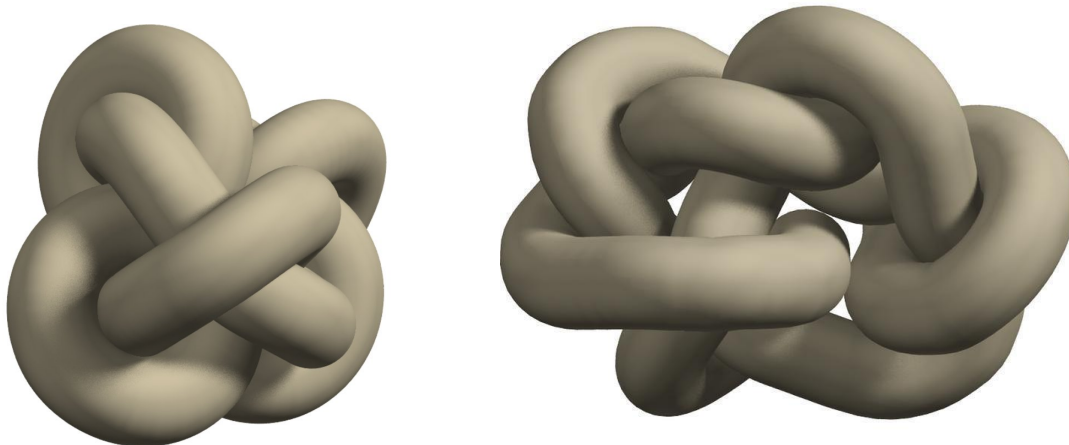


FIGURE 2. These two images of the 9_{20} knot show the tightest configurations obtained by our algorithm (left) and by the TOROS algorithm described in [47] (right). It is clear that our algorithm performs better once there are many self-contacts in the knot. In fact, the ropelength of the left-hand configuration is bounded by 80.2219, while the configuration on the right has ropelength bounded by 87.31.

authors used their condition to derive a ropelength critical configuration of the Borromean rings and a surprising ropelength critical configuration of a clasp formed by two tubes stretched across each other.

In each of these examples, the most difficult part of the result was the deduction of the structure of the set of self-contacts for the tight configuration. Since these contact maps are very sensitive to small perturbations of the centerline, it has been difficult to resolve them using previous numerical methods³. These contacts and the system of Lagrange multipliers on them are explicitly computed by our algorithm, allowing us to give medium-quality contact maps for a large number of knots and links. The contact maps offer some support for the hypothesis that a relatively small number of structures may reappear often in tight knots and links.

Previous work. This is not the first time gradient-like methods have been attempted for the knot-tightening problem. Our work has been inspired by Piotr Pieranski’s SONO algorithm [41], which follows a version of the length gradient, but does not include an explicit resolution of this vector against the active constraints. Our thinking is also informed by John Sullivan’s “energy-ropelength method” [52], which optimizes thickness instead of length, estimating the maximum diameter of a uniform embedded tube around the core curve by an L^p average of the radii of embedded cross-sectional disks and minimizing the resulting smooth functional using the conjugate-gradient implementation in Brakke’s `evolver` [5].

³The notable exception to this rule has been the “biarc” spline-annealing method of [14], which has produced well-resolved contact maps for the 3_1 and 4_1 knots.

2. A DISCRETIZATION FOR THE ROPELENGTH PROBLEM

Polygonal thickness. Consider a closed space polygon \mathcal{V} with vertices v_1, \dots, v_V and edges e_1, \dots, e_V . We will think of \mathcal{V} as the vector (v_1, \dots, v_V) in $(\mathbb{R}^3)^V = \mathbb{R}^{3V}$, and assume that all subscripts on vertices and edges are taken mod V . The unit tangent vector T_i to each edge of a polygon is well-defined on the interior of the edge. At the vertex v_i joining edges e_{i-1} and e_i , there are two tangent vectors T_{i-1} and T_i . The curvature of \mathcal{V} at v_i is usually thought of as a delta function whose mass is given by the turning angle θ_i from T_{i-1} to T_i . We will use a somewhat different definition of curvature for polygons:

Definition 2.1. The minimum radius of curvature (or MinRad) of \mathcal{V} at v_i is given by the radius of the unique circle that is tangent to the two edges meeting at v_i and that touches the midpoint of the shorter one.

Rawdon has shown [44] that if θ_i is the turning angle of \mathcal{V} at v_i , then we can give $\text{MinRad}(v_i)$ (and define $\text{MinRad}^\pm(v_i)$) by the expressions:

$$(1) \quad \frac{\min\{|e_{i-1}|, |e_i|\}}{2 \tan(\theta_i/2)} = \min \left\{ \frac{|e_{i-1}|}{2 \tan(\theta_i/2)}, \frac{|e_i|}{2 \tan(\theta_i/2)} \right\} = \min\{\text{MinRad}^-(v_i), \text{MinRad}^+(v_i)\}.$$

It is clear that while $\text{MinRad } v_i$ is not necessarily a differentiable function, the two functions $\text{MinRad}^\pm v_i$ are differentiable when they are defined. The motivation for this definition is that we can round off all the corners of \mathcal{V} by splicing in these circle arcs, generating a $C^{1,1}$ curve with radii of curvature equal to the $\text{MinRad}(v_i)$. We could have defined $\text{Thi}_p(\mathcal{V})$ to be the thickness of this curve. It turns out, however, that there is no closed form computation for that number (though it can be computed approximately, as we will see in Section 5).

We now define a set corresponding to dcsd for polygons:

Definition 2.2. Let $\text{dcsd}(\mathcal{V})$ be the set of (p, q) on \mathcal{V} with $p \neq q$ which are local minima of the self-distance function on \mathcal{V} .

There are several possible cases for (p, q) in $\text{dcsd}(\mathcal{V})$, since the polygon might have a vertex at one or both of the endpoints of the chord. These are shown in Figure 3.

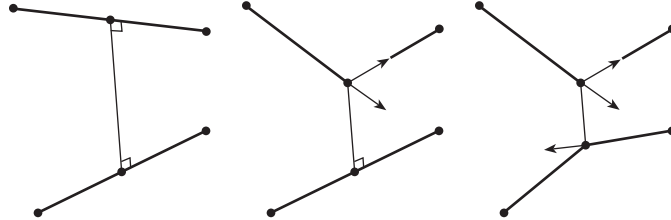


FIGURE 3. We see three types of local minima of the self-distance function on a space polygon \mathcal{V} in the three-dimensional drawings above. From left to right, these are an *edge-edge* pair, a *vertex-edge* pair, and a *vertex-vertex* pair.

We can then define Rawdon's polygonal thickness:

Definition 2.3. The polygonal thickness $\text{Thi}_p(\mathcal{V})$ of a space polygon \mathcal{V} without self-intersections is given by the minimum of

$$\text{Thi}_p(\mathcal{V}) := \min \left\{ \min_i \text{MinRad}(v_i), \min_{(p,q) \in \text{dcsd}(\mathcal{V})} \frac{d(p,q)}{2} \right\}.$$

We have carefully constructed this definition so that when polygons \mathcal{V}_n with increasing numbers of edges are inscribed in a space curve γ under some mild geometric hypotheses, $\text{Thi}_p(\mathcal{V}_n) \rightarrow \text{Thi}(\gamma)$ [44, 45, 47].

The problem with Thi_p . Definition 2.3 allows us to define the set of polygons with $\text{Thi}_p(\mathcal{V}) \geq 1$ as the polygons obeying a family of constraints in the form $\text{MinRad}(v_i) \geq 1$ and $d(p,q) \geq 2$ for $(p,q) \in \text{dcsd}(\mathcal{V})$. This is almost the standard form for constrained optimization problems:

$$(2) \quad \min_{\mathcal{V} \in \mathbb{R}^{3V}} f(\mathcal{V}) \text{ subject to } g_i(\mathcal{V}) \geq 0,$$

where f and the g_i are differentiable. The problem is that the set of constraint functions $d(p,q)$ for $(p,q) \in \text{dcsd}(\mathcal{V})$ depends on the polygon. We will need a common set of constraint functions for all polygons in a neighborhood of a solution.

Constraint thickness. To solve this problem, we will define a new thickness measure for polygons called *constraint thickness* which is given in the form above. We will then prove that for equilateral polygons, the new constraint thickness defines the same set of polygons as the old polygonal thickness.

We first define a subset of the pairs of points on a polygon

Definition 2.4. For a given positive τ and ℓ , let $\theta(\tau, \ell)$ be the turning angle of a pair of edges of length ℓ with $\text{MinRad} = \tau$. We set

$$\text{VB}(\tau, \ell) = \left\{ (p, q) \in \mathcal{V} \times \mathcal{V} : \text{vb}(p, q) \geq \frac{\pi}{\theta(\tau, \ell)} \right\},$$

where $\text{vb}(p, q)$ is the smaller number of vertices between points p and q (counting p and/or q if they are vertices) if they are on the same connected component of \mathcal{V} and ∞ otherwise.

We note that an easy computation shows that $\theta(\tau, \ell) = 2 \arctan(\ell/2\tau)$. We can now define our new thickness measure

Definition 2.5. The (τ, ℓ) -constraint thickness $\text{CThi}(\tau, \ell, \mathcal{V})$ of a polygon \mathcal{V} is given by

$$(3) \quad \text{CThi}(\tau, \ell, \mathcal{V}) = \min \left\{ \min_i \frac{\text{MinRad}(v_i)}{\tau}, \min_{(p,q) \in \text{VB}(\tau, \ell)} \frac{d(p,q)}{2} \right\}.$$

We note that \mathcal{V} need not be equilateral or have edglength ℓ to define the constraint thickness to defined the constraint thickness of \mathcal{V} . We can view τ as the ‘‘stiffness’’ of the rope (c.f. the

definition of λ -thickness in [9] and [7]), as it provides a lower bound on the radius of curvature of a tube of unit radius. Though our theory (and our code) should work for any $\tau \geq 1$, we have not experimented with values for τ other than 1 and so will write the $(1, \ell)$ -constraint thickness $\text{CThi}(1, \ell, \mathcal{V})$ as $\text{CThi}(\ell, \mathcal{V})$.

We can now prove that $\text{CThi}(\ell, \mathcal{V})$ is an equivalent thickness to Thi_p for equilateral polygons of edgelenh ℓ .

Theorem 2.6. *If \mathcal{V} is an equilateral polygon of edgelenh ℓ , $\text{Thi}_p(\mathcal{V}) \geq 1 \iff \text{CThi}(\ell, \mathcal{V}) \geq 1$.*

To prove the theorem we will need a lemma (c.f. Lemma 13 of [46]):

Lemma 2.7. *If \mathcal{V} is an equilateral polygon of edgelenh ℓ and $\text{MinRad} \geq \tau$, then $\text{dcsd}(\mathcal{V}) \subset \text{VB}(\tau, \ell)$.*

Proof. The proof has two parts — in the first, we show that the shorter arc between any $(p, q) \notin \text{VB}(\tau, \ell)$ has total curvature t less than π , while in the second we will show that any pair joined by such an arc cannot be in $\text{dcsd}(\mathcal{V})$. So suppose that $t \geq \pi$. We will prove that $(p, q) \in \text{VB}(\tau, \ell)$.

Since $\text{MinRad}(\mathcal{V}) \geq \tau$, we know that each turning angle of \mathcal{V} is less than $\theta(\tau, \ell)$. If the total curvature of the arc joining p and q is at least π , then $\text{vb}(p, q) \cdot \theta(\tau, \ell) \geq \pi$, so

$$(4) \quad \text{vb}(p, q) \geq \frac{\pi}{\theta(\tau, \ell)}$$

and $(p, q) \in \text{VB}(\tau, \ell)$, proving the claim.

Now suppose that $(p, q) \in \text{dcsd}(\mathcal{V})$. We claim that the total curvature t of each arc joining p and q is at least π , and hence that $(p, q) \in \text{VB}(\tau, \ell)$. Suppose not. The arc of \mathcal{V} joining p and q together with the chord from p to q form a closed space polygon \mathcal{V}' . The total curvature of this polygon is equal to t plus the turning angles at p and q . By Fenchel's Theorem [19], that total curvature is at least 2π . So the angle at p and the angle at q must sum to more than π . Thus either the angle at p or the angle at q must exceed $\pi/2$. But in that case, we could reduce $d(p, q)$ to first order by moving p or q along an edge from the arc which connects p and q , contradicting our assumption that $(p, q) \in \text{dcsd}(\mathcal{V})$. \square

We are now ready to prove Theorem 2.6:

Proof. Suppose that $\text{CThi}(\ell, \mathcal{V}) \geq 1$. This implies that $\min_i \text{MinRad}(v_i) \geq 1$ by the definition of CThi . Lemma 2.7 tells us that $\text{dcsd}(\mathcal{V}) \subset \text{VB}(1, \ell)$, so we know that

$$(5) \quad \min_{(p,q) \in \text{dcsd}(\mathcal{V})} d(p, q) \geq \min_{(p,q) \in \text{VB}(1, \ell)} d(p, q).$$

Together, these facts imply that $\text{Thi}_p(\mathcal{V}) \geq 1$, proving one direction of the theorem.

Suppose that $\text{Thi}_p(\mathcal{V}) \geq 1$. As above, this means that $\min_i \text{MinRad}(v_i) \geq 1$, so Lemma 2.7 applies and (5) holds. If the minimum in the right-hand side of (5) is achieved on the interior of

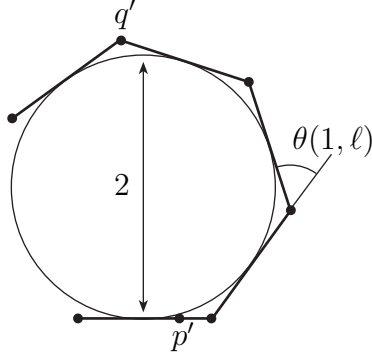


FIGURE 4. The key step in the proof of Theorem 2.6 is the proof that points p' and q' on an arc \mathcal{P} are at least distance 2 apart. This arc has equal edgelengths ℓ , each turning angle equal to $\theta(1, \ell) := 2 \arctan(\ell/2)$ and $n := \lceil \pi/\theta(1, \ell) \rceil$ edges. We see above that these conditions imply that \mathcal{P} has an inscribed circle of unit radius. Further, the marked point q' must have a larger y -coordinate than the top of the circle, providing the required lower bound on the distance from p' to q' .

$\text{VB}(1, \ell)$, then it is a local minimum of $d(p, q)$ where $p \neq q$ and so is in $\text{dcsd}(\mathcal{V})$. In this case, (5) is an equality and $\text{CThi}(\ell, \mathcal{V}) \geq 1$, completing the proof.

We are left with the case where the minimum of $d(p, q)$ over $\text{VB}(1, \ell)$ is realized by some (p, q) on the boundary of $\text{VB}(1, \ell)$. We claim that $d(p, q)/2 \geq 1$. This will complete the proof that $\text{CThi}(\ell, \mathcal{V}) \geq 1$.

By definition, (p, q) is on the boundary of $\text{VB}(1, \ell)$ only if $\text{vb}(p, q) = \lceil \pi/\theta(1, \ell) \rceil$. And since $\text{vb}(p, q)$ is constant on the interiors of edges, one of p and q (without loss of generality, q) must be a vertex. Since each turning angle of the arc of \mathcal{V} between p and q is bounded by $\theta(1, \ell)$, Schur's theorem [15] implies that $d(p, q)$ is bounded below by the distance between the endpoints of p', q' of a planar polygonal arc \mathcal{P} with the same edgelengths and each turning angle equal to $\theta(1, \ell)$. We depict the situation in Figure 4.

We know that \mathcal{P} has $n = \text{vb}(p, q)$ edges and total curvature $(n-1)\theta(1, \ell)$. Since $n = \text{vb}(p, q) = \lceil \pi/\theta(1, \ell) \rceil$, we have

$$(6) \quad n - 1 < \frac{\pi}{\theta(1, \ell)} \leq n \quad \text{so} \quad (n - 1)\theta(1, \ell) < \pi \leq n\theta(1, \ell).$$

Thus if we add an edge to \mathcal{P} at q' with turning angle $\theta(1, \ell)$ to form an arc \mathcal{P}^+ , the total curvature of \mathcal{P} is less than π while the total curvature of \mathcal{P}^+ is at least π . These facts imply that if the first edge of \mathcal{P} lies along the x -axis, the point q' has the largest y coordinate on \mathcal{P}^+ . But our turning angle and edgelength conditions imply that \mathcal{P}^+ has an inscribed circle of unit radius, so the y -coordinate of q' is at least two. This implies that $d(p', q') \geq 2$, completing the proof. \square

These proofs imply an obvious corollary which will be useful in practice:

Corollary 2.8. *If $\text{dcsd}(\mathcal{V}) \subset \text{VB}(\tau, \ell)$ and the distance between any two vertices on the boundary of VB is strictly greater than $\text{Thi}_p(\mathcal{V})$, then $\text{CThi} = \text{Thi}_p$ for polygons in a neighborhood of \mathcal{V} (regardless of whether or not \mathcal{V} is equilateral with edglength ℓ).*

Proof. The argument is the same as that of Theorem 2.6, using the hypotheses instead of Lemma 2.7 and the argument about turning angles. \square

Struts and Kinks. In our definition of Thi_p , we saw that pairs of points in dcsd and vertices with minimum MinRad were in control of thickness. We now want to develop similar sets of “controlling” pairs of points and vertices for CThi . This will require a bit of care.

Given any two line segments e_1 and e_2 in space, a calculation reveals that the minimum distance between them is attained at a single point unless e_1 and e_2 are parallel. In that case, the minimum is attained at an interval of corresponding pairs (as in Figure 5). The endpoints of these intervals are self-distances measured from an endpoint of one segment to a point on the other. Following this line of argument we see that for any space polygon the local minima of the self-distance function $d(p, q)$ are isolated unless there are pairs of parallel edges, in which case there may be families of local minima as above. Using these observations we define

Definition 2.9. The *strut set* $\text{Strut}(\mathcal{V})$ is the set of pairs (p, q) in $\text{VB}(1, \ell)$ with $d(p, q)/2 = 1$ and either

- (p, q) is an isolated local minimum of $d(p, q)$, or
- (p, q) is an *endpoint* of a family of local minima of $d(p, q)$.

In the second case, (p, q) must be a vertex-edge pair joining two parallel edges of \mathcal{V} .

We note that $\text{Strut}(\mathcal{V})$ is a finite subset of $\text{dcsd}(\mathcal{V})$ (which may be infinite if two edges are parallel). It is much easier to define

Definition 2.10. The *kink set* $\text{Kink}(\mathcal{V})$ is the set of vertices v_i and signs \pm with $\text{MinRad}^\pm v_i = 1$.

The strut and kink sets are both empty if $\text{CThi}(\ell, \mathcal{V}) > 1$.

Polygon space and variations of CThi . We now want to describe the space of variations of a polygon which preserve or increase CThi to first order. Given a polygon $\mathcal{V} \in \mathbb{R}^{3V}$ we can define a variation of \mathcal{V} by any $W = (w_1, \dots, w_V) \in \mathbb{R}^{3V}$. This variation generates a family of polygons

$$(7) \quad \mathcal{V}_t = \mathcal{V} + tW = (v_1 + tw_1, \dots, v_V + tw_V).$$

We now want to prove that $\text{CThi}(\ell, \mathcal{V})$ has a one-sided derivative as we vary \mathcal{V} according to any variation W and to give a finite procedure for computing that variation. This will require some setup.

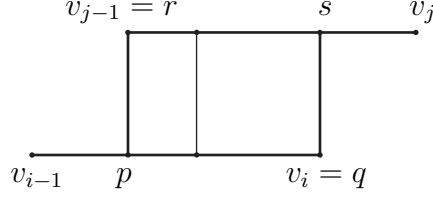


FIGURE 5. When the edges e_i and e_j are parallel, many chords realize the minimum distance between the segments. In this case, we show that the minimum derivative of distance between any of these pairs occurs at one end or the other. We name the endpoints of this family of chords p and q on e_i and r and s on e_j . One of each of these pairs must be an endpoint — in this case it is $q = v_i$ and $r = v_{j-1}$ that are endpoints.

Proposition 2.11. *Suppose that $\text{CThi}(\ell, \mathcal{V}) = 1$. Then viewing every pair of points (p, q) on \mathcal{V} and every $\text{MinRad}^\pm v_i$ as functions of t , the forward time derivative below exists and satisfies*

$$(8) \quad D_W \text{CThi}(\ell, \mathcal{V}) = \left. \frac{d}{dt^+} \text{CThi}(\mathcal{V}_t) \right|_{t=0} \\ = \min \left\{ \min_{(v_i, \pm) \in \text{Kink}} \left. \frac{d}{dt^+} (\text{MinRad}^\pm v_i)(t) \right|_{t=0}, \min_{\text{Strut}(\mathcal{V})} \left. \frac{d}{dt^+} \frac{d(p(t), q(t))}{2} \right|_{t=0} \right\}.$$

Proof. We begin by ignoring any $\text{MinRad} v_i$ functions which are not defined (which happens when v_{i-1}, v_i and v_{i+1} are colinear). Since $\text{CThi}(\ell, \mathcal{V})$ is equal to 1, the MinRad of these vertices will not affect $\text{CThi}(\mathcal{V} + tW)$ for small enough t . The function CThi is then the minimum of a set of differentiable functions $\text{MinRad}^\pm v_i$ and $d(p,q)/2$ indexed by the (compact) disjoint union of compact sets $\{v_1, \pm\} \sqcup \dots \sqcup \{v_V, \pm\} \sqcup \text{VB}(1, \ell)$ (where we assume that any v_i with $\text{MinRad} v_i$ undefined are missing). Clark's theorem for min-functions [16] tells us immediately that the derivative in (8) exists.

However, Clark's theorem tells us that

$$D_W \text{CThi}(\ell, \mathcal{V}) = \min \left\{ \min_{\substack{(v_i, \pm) \\ \text{MinRad}^\pm v_i = 1}} \left. \frac{d}{dt^+} \right|_{t=0} (\text{MinRad}^\pm v_i)(t), \min_{\substack{(p,q) \in \text{VB}(1, \ell) \\ d(p,q)/2 = 1}} \left. \frac{d}{dt^+} \right|_{t=0} \frac{d(p(t), q(t))}{2} \right\}.$$

The first set $\{(i, \pm) \mid \text{MinRad}^\pm v_i = 1\}$ is the kink set, which matches (8). But if a pair of edges in \mathcal{V} are parallel and at distance 2 from one another, then $\text{Strut}(\mathcal{V})$ is only a subset of $\{(p, q) \in \text{VB}(1, \ell) \mid d(p,q)/2 = 1\}$. We must prove that

$$(9) \quad \min_{\substack{(p,q) \in \text{VB}(1, \ell) \\ d(p,q)/2 = 1}} \left. \frac{d}{dt^+} \frac{d(p(t), q(t))}{2} \right|_{t=0} = \min_{(p,q) \in \text{Strut}(\mathcal{V})} \left. \frac{d}{dt^+} \frac{d(p(t), q(t))}{2} \right|_{t=0}.$$

For any pair of parallel edges with distance 2, we may assume that the situation is as in Figure 5. We label points p, q, r and s as in the Figure, and parametrize the line segments between p and q and between r and s by $\eta \in [0, 1]$. The pairs with $\eta = 0$ and $\eta = 1$ are in the strut set of \mathcal{V} , but the

pairs given by all other values of η are not. To prove (9) we must find

$$\min_{\eta \in [0,1]} \frac{d}{dt^+} \|\eta p + (1 - \eta)q - \eta r - (1 - \eta)s\|,$$

and show that it is attained at $\eta = 0$ or $\eta = 1$. If we view $p, q, r,$ and s as functions of time, then for any given η , the time derivative of the corresponding length is given by

$$\frac{1}{2} \langle \eta p + (1 - \eta)q - \eta r - (1 - \eta)s, \eta p' + (1 - \eta)q' - \eta r' - (1 - \eta)s' \rangle,$$

where we have used the fact that $d(e_i, e_j)/2 = 1$. Regrouping, we can rewrite this as

$$\frac{1}{2} \langle \eta(p - r) + (1 - \eta)(q - s), \eta(p - r)' + (1 - \eta)(q - s)' \rangle,$$

and using the fact that $p - r = q - s$ at time 0, we can again rewrite this as

$$\eta \langle p - r, p' - r' \rangle + (1 - \eta) \langle q - s, q' - s' \rangle.$$

Now as η varies between 0 and 1, we note that the η derivative of the above quantity is

$$\langle p - r, p' - r' \rangle - \langle q - s, q' - s' \rangle.$$

In particular, this derivative is nonzero for all $\eta \in [0, 1]$ unless $\langle p - r, p' - r' \rangle = \langle q - s, q' - s' \rangle$, in which case it vanishes identically. This means that the minimum value of this expression is always realized when $\eta = 0$ or $\eta = 1$. This completes the proof. \square

We can use Proposition 2.11 to define two sets of variations that will be of particular interest to us. The first set consists of variations that are tangent to the boundary or pointing into the interior of the set of polygons $C\text{Thi}(\ell, \mathcal{V}) \geq 1$. We will allow our polygons to move in these directions.

Definition 2.12. Suppose we have a polygon \mathcal{V} and a variation W of \mathcal{V} . If $C\text{Thi}(\ell, \mathcal{V}) = 1$, we say W is an *infinitesimal motion* of \mathcal{V} if the forward directional derivative

$$(10) \quad D_W C\text{Thi}(\ell, \mathcal{V}) \geq 0.$$

If $C\text{Thi}(\ell, \mathcal{V}) > 1$, we call every variation W an infinitesimal motion. The set of all infinitesimal motions of \mathcal{V} is denoted $I(\mathcal{V})$.

The following Corollary follows directly from Proposition 2.11.

Corollary 2.13. *The set $I(\mathcal{V})$ is the dual cone of the set $-\nabla^{d(p,q)/2}$ for $(p, q) \in \text{Strut}(\mathcal{V})$ and $-\nabla \text{MinRad}^\pm v_i$ for $(v_i, \pm) \in \text{Kink}(\mathcal{V})$.*

Proof. We need only recall that the dual cone A^+ to a set of vectors A is the set of vectors X for which $\langle X, W \rangle \leq 0$ for all $W \in A$. Since the directional derivatives of $d(p,q)/2$ and $\text{MinRad}^\pm v_i$ in the direction X are the dot products of X with $-\nabla^{d(p,q)/2}$ and $-\nabla \text{MinRad}^\pm v_i$, X is in the dual cone if and only if all these directional derivatives are nonnegative. But by the Proposition, this implies that $D_X C\text{Thi}(\ell, \mathcal{V})$ is nonnegative as well. \square

The second set of variations of interest will be the normal cone of the boundary of the set of polygons with $C\text{Thi}(\ell, \mathcal{V}) \geq 1$. We will forbid our polygons from moving in these directions.

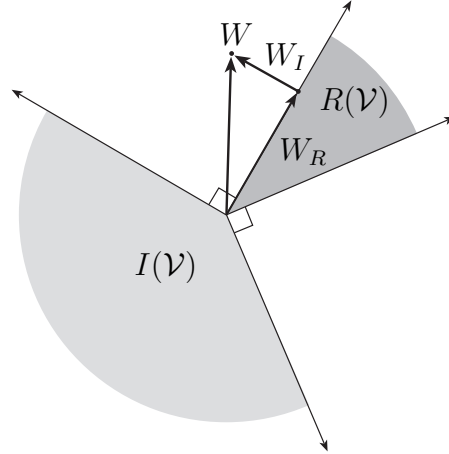


FIGURE 6. The infinitesimal motions $I(\mathcal{V})$ and the resolvable motions $R(\mathcal{V})$ of \mathcal{V} form dual convex cones. Hence, although these are not orthogonal subspaces of \mathbb{R}^{3V} , a similar decomposition property holds true: any vector W may be written uniquely as a sum of a vector $W_I \in I(\mathcal{V})$ and a vector $W_R \in R(\mathcal{V})$.

Definition 2.14. The convex cone of *resolvable motions* $R(\mathcal{V})$ of \mathcal{V} is the cone generated by the set $-\nabla^{d(p,q)/2}$ for $(p, q) \in \text{Strut}(\mathcal{V})$ and $-\nabla \text{MinRad}^\pm v_i$ for $(v_i, \pm) \in \text{Kink}(\mathcal{V})$. $R(\mathcal{V})$ is the set of vectors $R \in \mathbb{R}^{3V}$ which can be expressed in the form

$$(11) \quad R = \sum_{(p,q) \in \text{Strut}(\mathcal{V})} -\lambda_i^2 \nabla \frac{d(p,q)}{2} + \sum_{v_j \in \text{Kink}(\mathcal{V})} -\lambda_j^2 \nabla \text{MinRad } v_j.$$

Here the indices i and j just number the elements of the strut and kink sets. The constants λ_i^2 and λ_j^2 are nonnegative numbers, as suggested by the notation.

It is a standard fact from optimization theory that $R(\mathcal{V}) = I(\mathcal{V})^+$, since for any set of vectors $\{v\}$ the double dual $\{v\}^{++}$ is the cone generated by $\{v\}$.

Theory of constrained optimization. Given a function $f(\mathcal{V})$ on the space of polygons \mathbb{R}^{3V} , we can compute the negative gradient $-\nabla f$, which is a variation vector in \mathbb{R}^{3V} . We are now interested in understanding how this gradient is modified by the constraint $\text{CThi}(\ell, \mathcal{V}) \geq 1$. This thickness constraint models the effect of an embedded tube around the polygon: it allows some motions of \mathcal{V} and blocks others.

Definition 2.15. The *constrained gradient* $(-\nabla f)_I$ of $-f$ is the closest vector in $I(\mathcal{V})$ to $-\nabla f(\mathcal{V})$.

We now recall that any convex cone and its dual cone provide a kind of orthogonal decomposition of their ambient vector space, as shown in Figure 6.

Proposition 2.16 ([51], Thm. 2.8.7). *Any vector $W \in \mathbb{R}^{3V}$ may be uniquely written*

$$(12) \quad W = W_R + W_I, \quad \text{where } \langle W_R, W_I \rangle = 0,$$

$W_R \in R(\mathcal{V})$ is the closest resolvable motion to W , and $W_I \in I(\mathcal{V})$ is the closest infinitesimal motion to W .

We note that this Proposition shows that the constrained gradient of $-f$ is well-defined. Further, it is easy to show that the constrained gradient is the direction of steepest descent for f within $I(\mathcal{V})$. This makes us guess that the constrained gradient should vanish at a critical point for minimizing f . To prove it, we define critical points more carefully

Definition 2.17. We say that \mathcal{V} is *thickness-critical for minimizing f* if either:

- $D_W f = 0$, or
- $\text{CThi}(\ell, \mathcal{V}) = 1$ and for any W with $D_W f(\mathcal{V}) < 0$, we have $D_W \text{CThi}(\ell, \mathcal{V}) < 0$.

In the first case, we are at an unconstrained critical point of the objective function f . In the second, we are at a constrained critical point where motion in the direction of the negative gradient of f is blocked by active constraints. We then have a version of the Kuhn-Tucker theorem (restated in our language from the original form in [10]), which gives a verifiable condition for thickness-criticality.

Theorem 2.18. *The polygon \mathcal{V} is thickness-critical for minimizing $f \iff -\nabla f$ is in $R(\mathcal{V}) \iff$ the constrained gradient $(-\nabla f)_I$ vanishes.*

Proof. It suffices to show that the first two statements are equivalent, since the second and third are clearly equivalent by Proposition 2.16.

If $-\nabla f$ is not in $R(\mathcal{V})$, then Farkas' theorem implies that there exists some W with $\langle W, \nabla f \rangle = D_W f < 0$ and $\langle W, R \rangle \leq 0$ for all $R \in R(\mathcal{V})$ ([40], p. 118). Using the definition of $R(\mathcal{V})$ and Proposition 2.11, this implies $D_W \text{CThi}(\ell, \mathcal{V}) \geq 0$. Thus \mathcal{V} is not thickness-critical for minimizing f .

If $-\nabla f$ is in $R(\mathcal{V})$ we will prove that \mathcal{V} is thickness-critical for minimizing f . We first observe that the dual cone of $-\nabla f$ contains the dual cone $R^+(\mathcal{V})$. Now suppose we have some W with $D_W f < 0$. Then $\langle W, -\nabla f \rangle > 0$, so $W \notin (-\nabla f)^+$ and in particular $W \notin R^+(\mathcal{V})$. But this means that $\langle W, R \rangle > 0$ for some $R \in R(\mathcal{V})$, so $D_W \text{CThi}(\ell, \mathcal{V}) < 0$. Hence \mathcal{V} is thickness-critical for minimizing f . \square

We can give a natural interpretation of this Theorem in mathematical and physical terms by considering the condition $-\nabla f \in R(\mathcal{V})$. By definition, this means that

$$(13) \quad -\nabla f + \sum_{(p,q) \in \text{Strut}(\mathcal{V})} \lambda_i^2 \nabla \frac{d(p,q)}{2} + \sum_{v_j \in \text{Kink}(\mathcal{V})} \lambda_j^2 \nabla \text{MinRad } v_i = 0.$$

Mathematically, the λ_i^2 and λ_j^2 are Lagrange multipliers. If we think of the thickness constraint as an embedded tube around \mathcal{V} , we can interpret these scalars as magnitudes of compression forces transmitted by tube contacts (for struts) and angles where the polygon resists further bending (for kinks).

In general, we cannot expect every local minimum of a constrained function to be a constrained critical point in the sense of Definition 2.17. If the set of polygons defined by $\text{CThi}(\ell, \mathcal{V})$ had an outward-pointing cusp we might reach a point where some W with $D_W f < 0$ had $D_W \text{CThi} = 0$. For example, the constrained system

$$\text{minimize } f(x, y) = -x, \text{ subject to } g(x, y) = \min\{x^3 - y, y\} \geq 0$$

has this property at the local minimum $(0, 0)$ for $W = (1, 0)$. The problem here is simply that $D_W g \leq 0$ for all W . This does not happen for thickness-constrained polygons, but we will need another idea to prove it:

Definition 2.19. We say that \mathcal{V} is *constraint-qualified* (in the sense of Mangasarian and Froylovitz [35]) if there exists some W so that $D_W \text{CThi} > 0$.

It is then standard to show

Proposition 2.20 ([10]). *Any constraint-qualified local minimum of f is a thickness-critical point for minimizing f .*

In our case, scaling \mathcal{V} provides the desired motion, so we have

Corollary 2.21. *If the polygon \mathcal{V} is a local minimum for f , then it is a thickness-critical point for minimizing f .*

We make a final note that in general, our criticality theory works equally well for CThi and Thi_p (even for polygons \mathcal{V} which are not equilateral), as long as they obey the hypotheses of Corollary 2.8. This is true in practice in all of our numerically computed configurations.

3. BRIDGING THEORY AND COMPUTATION

Overview of the algorithm. We have now derived enough theory to describe our algorithm in general terms. We wish to minimize the function $\text{Len}(\mathcal{V})$ subject to the constraint $\text{CThi}(\ell, \mathcal{V}) \geq 1$. We will do so by computing the constrained gradient $(-\text{Len } \mathcal{V})_I$ and stepping in this direction. These steps will reduce $\text{Len}(\mathcal{V})$ while keeping \mathcal{V} close to the set $\text{CThi}(\ell, \mathcal{V}) \geq 1$ (since the constraints are nonconvex, we cannot stay entirely inside this set). When $(-\text{Len } \mathcal{V})_I$ vanishes, the algorithm will terminate. By Theorem 2.18 if the constrained gradient was exactly zero, the resulting configuration would be a thickness-critical point for minimizing length. We note that our algorithm will attempt to maintain an approximately equilateral polygon \mathcal{V} but it is not required to: constant edglength ℓ is not a hypothesis of Theorem 2.18. Our only caveat is that we must remember that $\text{CThi}(\mathcal{V})$ may not be equal to $\text{Thi}_p(\mathcal{V})$ if the final configuration fails to obey the hypotheses of Corollary 2.8. We also note that there is nothing special about choosing $\text{Len}(\mathcal{V})$ as the function to minimize — both our theory and our code would work just as well for any other function.

Computing the constrained gradient. To implement this algorithm, we must be able to compute the constrained gradient $(-\nabla f)_I$. This is a standard problem in linear algebra. By definition, if

$-\nabla f$ is written as $(-\nabla f)_R + (-\nabla f)_I$ using Proposition 2.16, the constrained gradient is equal to $(-\nabla f)_I$. We can compute that by computing $(-\nabla f)_R$, which is easy to do since we know the generators of the cone $R(\mathcal{V})$.

Definition 3.1. If $\text{CThi}(\ell, \mathcal{V}) = 1$, the *rigidity matrix* A of \mathcal{V} is the matrix whose columns are the gradients $-\nabla^{d(p,q)/2}$ for $(p, q) \in \text{Strut}(\mathcal{V})$ and $-\nabla \text{MinRad}^\pm v_i$ for $(v_i, \pm) \in \text{Kink}(\mathcal{V})$.

We can construct the rigidity matrix by finding the members of $\text{Strut}(\mathcal{V})$ and $\text{Kink}(\mathcal{V})$. It follows from the definition that $R(\mathcal{V})$ is the image of the positive orthant under the matrix A . By Proposition 2.16, $(-\nabla f)_R$ is the closest vector in that image to $-\nabla f$. So if we solve the non-negative least-squares (NNLS) problem

$$(14) \quad \min_{\Lambda \geq 0} \|A\Lambda - (-\nabla f)\|,$$

then $(-\nabla f)_R = A\Lambda$ and $(-\nabla f)_I = -\nabla f - A\Lambda$. This least-squares problem is a special kind of quadratic programming problem which has been well-studied in numerical linear algebra (see [4]). In our case, the problem is much easier because A is extremely sparse — the gradients of the $d(p,q)/2$ involve no more than 4 vertices (and so 12 variables), while the gradients of the MinRad^\pm involve only 3 vertices (and 9 variables). So each column of A , which is typically 1000 or more entries long, contains at most 12 nonzero entries.

The gradient of Length. We can now compute $(-\nabla \text{Len})_I$ if we can compute $-\nabla \text{Len}$, build the rigidity matrix A from the strut and kink sets, and solve the NNLS problem in (14). We will take these problems in order.

Length is a differentiable function of polygons $\mathcal{V} \in \mathbb{R}^{3V}$, whose gradient is given by a straightforward calculation:

Proposition 3.2. *The gradient of length of a polygon \mathcal{V}_n is given by the collection of n vectors*

$$(15) \quad \nabla \text{Len}(\mathcal{V})_k = \frac{v_{k-1} - v_k}{\|v_{k-1} - v_k\|} + \frac{v_{k+1} - v_k}{\|v_{k+1} - v_k\|}.$$

The gradient of $d(p,q)/2$. Given a pair of points (p, q) on \mathcal{V} , the gradient of the distance between them is a set of four vectors located at the endpoints of the edges on which p and q lie. These vectors are given by a calculation:

Proposition 3.3. *Suppose that $(p, q) \in \text{Strut}(\mathcal{V})$. If $p = \alpha v_i + (1 - \alpha)v_{i+1}$ and $q = \beta v_j + (1 - \beta)v_{j+1}$ then*

$$\nabla \frac{d(p, q)}{2} = \frac{1}{2d(p, q)} \{ \alpha(p - q), (1 - \alpha)(p - q), \beta(q - p), (1 - \beta)(q - p) \}.$$

where these three vectors are applied to v_i, v_{i+1}, v_j and v_{j+1} in order.

The gradient of MinRad^\pm . As we noted above, the MinRad^\pm are differentiable where they are defined. We now compute the gradient on MinRad^+ , noting that the gradient of MinRad^- is similar.

Proposition 3.4. Given a vertex i on \mathcal{V}_n with finite $\text{MinRad}^\pm(v_i)$, we let n denote the oriented normal vector to the plane defined by v_{i-1}, v_i, v_{i+1} and define the scalar constant

$$K = \frac{\|v_{i+1} - v_i\|}{2 \cos \theta - 2}$$

and the vector constants

$$V = \frac{v_{i+1} - v_i}{2 \tan(\theta/2) \|v_{i+1} - v_i\|}, \quad W = K \frac{(v_{i-1} - v_i) \times n}{\|v_{i-1} - v_i\|^2}, \quad X = K \frac{n \times (v_{i+1} - v_i)}{\|v_{i+1} - v_i\|^2}.$$

Then if we write the gradient of MinRad^+ as a triple of vectors located at v_{i-1}, v_i , and v_{i+1} we have

$$\nabla \text{MinRad}^+(v_i) = \{W, -W - X - V, X + V\}.$$

Proof. The proof is a lengthy calculation. We want to compute the gradient of $\text{MinRad}^+(v_i) = \frac{\|v_{i+1} - v_i\|}{2 \tan(\theta/2)}$, where θ is the turning angle at vertex v_i . We start with a change of variables. Let $A = v_{i-1} - v_i$ and $B = v_{i+1} - v_i$. We can rewrite MinRad^+ in terms of these variables and compute its gradient as follows:

$$(16) \quad \nabla \frac{\|B\|}{2 \tan(\theta/2)} = \frac{1}{2 \tan(\theta/2)} \left(0, \frac{B}{\|B\|} \right) - \frac{1}{2} \left[\frac{\|B\|}{\tan^2(\theta/2)} \cdot \frac{d}{d\theta} \tan(\theta/2) \right] \nabla \theta.$$

Now

$$(17) \quad \frac{d}{d\theta} \tan(\theta/2) = \frac{1}{2 \cos^2(\theta/2)} = \frac{1}{2 \frac{1 + \cos \theta}{2}} = \frac{1}{1 + \cos \theta}, \quad \text{and} \quad \tan^2(\theta/2) = \frac{1 - \cos \theta}{1 + \cos \theta}.$$

So we can rewrite (16) as

$$\nabla \frac{\|B\|}{2 \tan(\theta/2)} = \frac{1}{2 \tan(\theta/2)} \left(0, \frac{B}{\|B\|} \right) - \frac{\|B\|}{2 - 2 \cos \theta} \nabla \theta = (0, V) + K \nabla \theta.$$

Keeping track of the sign of the exterior angle, we see that if n is the oriented unit normal to the plane containing A and B , we have

$$\nabla \theta = \left(\frac{A \times n}{\|A\|^2}, \frac{n \times B}{\|B\|^2} \right) \quad \text{so} \quad \nabla \frac{\|B\|}{2 \tan(\theta/2)} = (W, X + V).$$

Using the definition of A and B to change back to the original variables completes the proof. \square

The function $\text{MinRad}(v_i)$ provides a discrete analog to the radius of curvature for the polygonal curve \mathcal{V} at v_i . Since this is a numerical computation of a second derivative, we expect the function to be quite sensitive to small changes in the positions of the vertices of \mathcal{V} . This sensitivity will limit the accuracy of our computations, so we record an estimate of the norm of the gradient of $\text{MinRad}^+(v_i)$.

Corollary 3.5. If \mathcal{V} is an equilateral polygon with edgelenh ℓ and $\text{MinRad } v_i = 1$ then

$$\|\nabla \text{MinRad}^\pm v_i\| \geq \frac{2}{\ell^2}.$$

Proof. Consider

$$\|W\| = \frac{\|v_{i+1} - v_i\| \|(v_{i-1} - v_i) \times n\|}{|2 \cos \theta - 2| \|v_{i-1} - v_i\|^2}.$$

Since the polygon is equilateral, and n is a unit vector normal to $v_{i-1} - v_i$, this is just $\|W\| = 1/|2 \cos \theta - 2|$. If $\text{MinRad} = 1$, then (squaring MinRad and using both half-angle formulae for tangent) we see that $\|W\| = |2 + 2 \cos \theta|/\ell^2$. Since W appears alone in the formula for ∇MinRad^+ , this is a lower bound for the norm of the entire gradient. \square

4. PROGRAM DESIGN

Issues of scale. The design and implementation of our algorithm `ridgerunner` were shaped by the scale of the knot-minimizing problems we intended to solve and the amount of computer power we had on hand to solve them. To inform the discussion that follows, we will now take a moment to consider the dimensions of our problems. In a typical run, we started by minimizing the length of a low-resolution version of our knot or link with 2 vertices per unit of ropelength (80 to 150 vertices). Once that configuration was minimized, a medium resolution run at 4 vertices per unit of ropelength was performed. A final run followed at 8 vertices per unit ropelength. Most of the runtime was spent during the final run, which took 20 – 40 CPU hours on a desktop computer. During the final run, the average edgelenh ℓ for our curves was approximately 0.061, which meant that there were 658 edges. The average size of the strut set was 919 pairs of points, while the average size of the kink set was 19 vertices. The rigidity matrix was then on average a 938×1974 matrix which was 99.4% sparse (no more than 11199 of its 1851612 entries were nonzero). A typical run contained several hundred thousand steps.

The algorithm. Our method is based loosely on the method of constrained gradient descent. The basic idea is to generate a series of polygons \mathcal{V}_i which converge to a limit polygon which is thickness-critical for minimizing a function $f(\mathcal{V})$ by taking a series of steps in the form

$$(18) \quad \mathcal{V}_{k+1} = \mathcal{V}_k + \alpha(-\nabla f)_I, \quad \text{where } \alpha \text{ is chosen by a search algorithm.}$$

When $\text{CThi}(\ell, \mathcal{V}) > 1$, this is just the method of steepest descent, since $(-\nabla f)_I = -\nabla f$. When $\text{CThi}(\ell, \mathcal{V}) = 1$, these steps are tangent to the boundary of $\text{CThi}(\ell, \mathcal{V}) \geq 1$ and in principle decrease CThi by no more than $O(\alpha^2)$. In some circumstances, such as when two sections of tube touch for the first time, we can decrease CThi by $O(\alpha)$ (which is much larger, since $\alpha \ll 1$). We control this error by searching for an α which keeps $\text{CThi}(\ell, \mathcal{V}_k + \alpha(-\nabla f)_I)$ within acceptable bounds. When $\text{CThi}(\ell, \mathcal{V}_k)$ becomes too small, we correct the accumulated error using a Newton's method-type solver. The code terminates when we the constrained gradient is small enough to convince us that we are near a point which is thickness-critical for minimizing f . This procedure is summarized in Algorithm 1.

In the rest of this section, we will comment on each of these steps in turn.

Algorithm 1: The outline of the `ridgerunner` algorithm.

input : A polygon \mathcal{V}_0 and an error bound MaxErr .
output: A sequence of positions \mathcal{V}_k with $\text{CThi}(\ell, \mathcal{V}_k) \geq 1 - \text{MaxErr}$.

- 1 **repeat**
- 2 Compute $-\nabla f = -\nabla \text{Len}(\mathcal{V}_k) + -\nabla \text{Eq}(\mathcal{V}_k)$;
- 3 Find $\text{Strut}(\mathcal{V})$ and $\text{Kink}(\mathcal{V})$ and construct the rigidity matrix A ;
- 4 Compute constrained gradient $(-\nabla f)_I$;
- 5 Search for α so that $\mathcal{V}_k + \alpha(-\nabla f)_I$ minimizes ropelength and is computationally acceptable and set $\mathcal{V}_{k+1} = \mathcal{V}_k + \alpha(-\nabla f)_I$;
- 6 **if** $\text{CThi}(\ell, \mathcal{V}_{k+1}) < 1 - \text{MaxErr}$ **then**
- 7 Correct $\text{CThi}(\ell, \mathcal{V}_{k+1})$ by Newton’s method;
- 8 **end**
- 9 **until** $\|(-\nabla f)_I\|/\|-\nabla f\|$ is sufficiently small;

Step 2. Equilateral polygons, CThi and Thi_p . We have only proved that $\text{CThi} \geq 1 \iff \text{Thi}_p \geq 1$ for equilateral polygons. It is therefore important that our \mathcal{V}_k remain at least approximately equilateral during a run. We enforce this constraint by defining a penalty function $\text{Eq}(\mathcal{V})$ which is minimized when \mathcal{V}_k is equilateral and minimizing the sum $\text{Len}(\mathcal{V}) + \text{Eq}(\mathcal{V})$. This is quite effective (a typical run recorded an average error in edglength of about 0.385%) in practice. We note that while CThi and Thi_p might not be equal for nonequilateral polygons, we avoid any problems that might result by performing all of our final ropelength calculations with respect to the original Thi_p thickness.

Step 3. Finding $\text{Strut}(\mathcal{V})$ and $\text{Kink}(\mathcal{V})$. In principle, the strut and kink sets could be found by direct inspection of all pairs of edges and all vertices of \mathcal{V} . But since there are usually 10^6 such pairs, this naive method consumes too much runtime. So to find the strut and kink sets, we used the clustering code `octrope` of Ashton and Cantarella described in [1]. This was fast enough that over 30 seconds of a typical⁴ run about 10% of runtime was spent finding $\text{Strut}(\mathcal{V})$ and $\text{Kink}(\mathcal{V})$. The algorithm in `octrope` does not take advantage of the fact that it is called successively on data which vary little between calls, so a much faster customized strut-finding code could be written into `ridgerunner`. However, these figures show that this project would have little impact on overall performance.

Step 4. Finding the constrained gradient. Once we have $\text{Strut}(\mathcal{V})$ and $\text{Kink}(\mathcal{V})$ we can use the gradient formulae given in Propositions 3.3 and 3.4 to construct the rigidity matrix A . We must then solve the sparse non-negative least squares (SNNLS) problem $\min_{\Lambda \geq 0} \|A\Lambda - (-\nabla f)\|$, which we recall as Equation 14 on page 16.

We use the freely available `tsnnls` library of Cantarella, Piatek, and Rawdon [12], which is an implementation of the block-pivoting algorithm of Portugal, Judice and Vicente [43]. The PJV algorithm solves a sequence of unconstrained least-squares problems to find a partition of

⁴a 400 edge 5.1 knot with about 600 struts

the variables of Λ into complementary sets F and G representing variables which will be nonzero and zero in the solution to (14). It is very important to take advantage of the sparsity of A in order to solve these (rather large) problems in an acceptable amount of time, as this step makes the dominant contribution to our overall runtime in most cases. To this end, `tsnnls` solves the least-squares problem $Ax = b$ by solving the “normal equations” $A^T Ax = A^T b$. Since $A^T A$ is symmetric, we can solve this system using a Cholesky factorization. This is done very quickly using the multifrontal supernodal sparse Cholesky code `TAUCS` of Toledo et al. [53].

We have sacrificed some accuracy in favor of speed, since the condition number of $A^T A$ is the square of the condition number of A . A standard “rule of thumb” in such situations is that the error in the solution is on the order of machine epsilon (10^{-16}) multiplied by condition number. To verify that this was small in practice, we used the `rcond` function in `LAPACK` to estimate the condition number of the rigidity matrices of all of our final configurations. The average condition number was on the order of 10^4 with none being worse than 8×10^5 . Thus we expect to have an average error on the order of 10^{-8} and a worst-case error of 10^{-6} in our final computations of the constrained gradient.

It is also worth noting that the `TAUCS` code will fail if the rigidity matrix is singular, which will occur when there is more than one way to balance gradient force. This is expected for very complicated knots, but seems to be rare among knots in our dataset. A more advanced version of `tsnnls` would calculate a minimum-norm solution to the least-squares problem in this case.

Step 5. Choosing a stepsize. When $C\text{Thi}(\mathcal{V}) > 1$ our code sets a small maximum stepsize of 10^{-2} and proceeds by Euler integration⁵. Once $C\text{Thi}(\mathcal{V}) = 1$, thickness typically decreases by a small amount on each step. We choose α by a line search algorithm, finding the minimum ropelength of configurations in the given direction using Brent’s method with a relatively low precision.

However, we do not always accept the ropelength-minimizing α . Instead, we apply a collection of ad hoc conditions which we describe as α being “computationally acceptable”. These include an upper bound on stepsize of 10^{-2} , a lower bound of 10^{-6} , and the requirement that the linear algebra solver of Step 4 can compute a new direction $-\nabla f_I$ at the new location. These are motivated by several practical considerations. If the stepsize is permitted to be too large, loose configurations will often form large kinked regions before the tube contacts itself. Kinks reduce stepsizes by orders of magnitude— in practice, this means that such a run takes an unacceptably long time to converge. If the stepsize is permitted to be too small, the solver can stall just before discovering a new self-contact. In these cases it has proved better to take the risk of a slight increase in ropelength in order to improve the strut set. Finally, even when the stepsize is less than 10^{-2} , if an arc of the knot suddenly contacts another arc, introducing too many new struts into the rigidity matrix, the matrix can become numerically singular, defeating the `tsnnls` solver of Step 4. Thus, we must look ahead and make sure the next position will be acceptable to `tsnnls` before locking in a stepsize.

⁵We could improve the accuracy and speed of this portion of the computation by using a smarter ODE solving method. But these steps have no linear algebra involved, so they are already orders of magnitude faster than the ones to come. In practice, this portion of the run consumes $< 1\%$ of the total runtime.

Step 7. Error correction. When the error bound $\text{MaxErr} = 10^{-4}$ is reached, we use Newton’s method to return \mathcal{V}_k to a configuration with larger thickness. For any given variation W of \mathcal{V} we can estimate the change in the $d^{(p,q)}/2$ for $(p, q) \in \text{Strut}(\mathcal{V})$ and in $\text{MinRad}^\pm v_i$ for $(v_i, \pm) \in \text{Kink}(\mathcal{V})$ by $A^T W$, where A is the rigidity matrix we have already computed.

We use this observation in a straightforward way. We construct a vector C of desired corrections which is equal to $(1 - \text{MaxErr}/2) - d^{(p,q)}/2$ for $(p, q) \in \text{Strut}(\mathcal{V})$ and $(1 - \text{MaxErr}/2) - \text{MinRad}^\pm v_i$ for $(v_i, \pm) \in \text{Kink}(\mathcal{V})$. Having done so, we find a minimum-norm solution to $A^T W = C$. We then step according to W , using a search algorithm to decide the stepsize, rebuild the rigidity matrix in case we have changed the strut or kink set in the correction step, and iterate.

We note that we do not attempt to correct all of the error in $C\text{Thi}(\mathcal{V})$ during this procedure. If we did so, we would risk losing struts and kinks when we rebuild the rigidity matrix. In that case, the next Newton step, ignoring those pairs or vertices, might rediscover them as struts and kinks. In principle, this cycling behavior could delay or prevent convergence of the Newton procedure, as noted by Fletcher [23]. Our method does not eliminate this possibility entirely (in the current version of the code, we have observed occasional failures of the Newton solver) but in practice the Newton solver almost always converges in only a few iterations.

The main problem with the Newton solver is that it is slow for large problems. The matrix A^T is mapping from a high-dimensional space of variations to a relatively low-dimensional space of struts and kinks, so it has a large kernel. Hence the matrix AA^T is not positive definite, and so we cannot solve $A^T W = C$ using the method of normal equations and the fast Cholesky decomposition of `TAUCS`. Instead, we must use the older `lsqr` code of Paige and Saunders [39] to find a minimum-norm solution to the problem. This can be very slow. For instance, in a 640 edge trefoil with 975 struts and 10 kinks, correction steps consumed anywhere between 3 and 25 seconds of runtime. Normal steps completed in less than a second. We always have the option of sidestepping Newton correction by simply scaling the knot (as in Pieranski’s `SONO` algorithm). This preserves ropelength but destroys the strut set completely, requiring us to rebuild the strut set during subsequent steps. Our experience has been that this can improve performance during the middle stages of a run, when a fairly large number of struts and kinks have formed but the knot is still far from tight, but it is better to use Newton correction in the final stages of a run when one is trying to adjust a converged strut set to improve the final results.

At the moment, the speed of `lsqr` controls the overall performance of our code. We hope to find an improved error-correction procedure in future versions of the software.

Modified versions of the algorithm. We have also modified our algorithm to handle some special cases, such as open curves with fixed endpoints or endpoints constrained to lie in planes. In these cases, the gradients of the endpoint constraints are added to the rigidity matrix and the gradient of length is resolved against them in Step 4. In addition, a specialized error-correction algorithm enforces the constraints after each step to prevent numerical error from causing the endpoints to drift away from their positions over time. The general Newton’s method algorithm for error-correction is also modified in these cases to take endpoint constraints into account.

In addition, we have found that curves whose final tight positions have long segments with no struts or kinks as well as tightly curved regions with many struts and kinks often take a very large number of steps to tighten completely. Sections of the curve with no struts or kinks simply minimize length with no constraints and must therefore end up as straight lines. But as they approach this position, the gradient of length approaches zero, while regions where the gradient of length is balanced by struts and kinks have comparatively large length gradients. Since the step size is controlled by the tightly curved regions, it may take a very long time for the strut and kink-free regions to finish straightening. We have had some success in these cases with a modified version of our algorithm which detects sections of curve with no struts or kinks and scales up the length gradient on those portions of the curve alone.

5. RESULTS OF COMPUTATIONS

We now present the main results of our computations. To summarize, we have significantly extended the range and quality of existing computations of tight knots and links. The new data support some interesting conjectures about the geometric structure of these configurations.

Validation of `ridgerunner` computations. To verify that the system works, we checked the results of `ridgerunner` against some theoretical results. The results of the comparison appear in Table 1. As we can see from the Table, the relative error in these ropelength computations is as small as 0.0017%.

The paper [10] also gives an explicit strut set for the Borromean rings. To compare the numerically computed strut set to the theoretical one, we plot them together in Figure 7. The Figure shows that the numerically computed strut set is quite close to the actual one. Figure 8 shows a similar comparison between theoretical results and a `ridgerunner` computation for the strut set of the “simple clasp” formed by two strands looped over one another. The theoretical results in [10] for this clasp assume that the curvature of the clasp is not bounded, so we compare with the results of a run of our software which did not enforce curvature constraints.

Computing polygonal ropelength minimizers for many knots and links. We minimized polygonal ropelength for all prime knots of 10 and fewer crossing and all prime links of 9 and fewer crossings (a total of 379 knot and link types) at resolutions of at least 8 vertices per unit of ropelength (several hundred vertices in total). For a few knots and links of special interest, we computed high resolution runs with 16, 32, or 74 vertices per unit ropelength. The largest runs in our dataset contain about 2400 vertices.

The computations were performed on clusters at the University of St. Thomas, the University of Georgia, and the ACCRE cluster at Vanderbilt University. We began our computations with an initial low-resolution (200 vertices or fewer) polygon, which we ran until the residual was sufficiently low. We then increased resolution by a minrad-preserving version of spline interpolation and minimized again from the resulting new starting configurations. Our initial goal was a residual less than 0.01, which we achieved for 375 of the 379 knots and links in our data set. We were able to reach

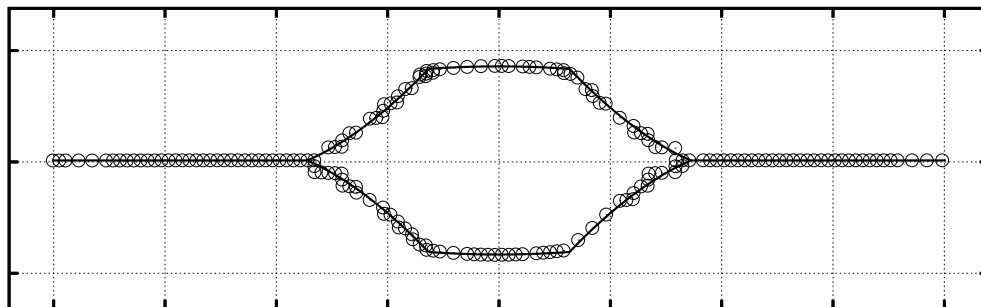
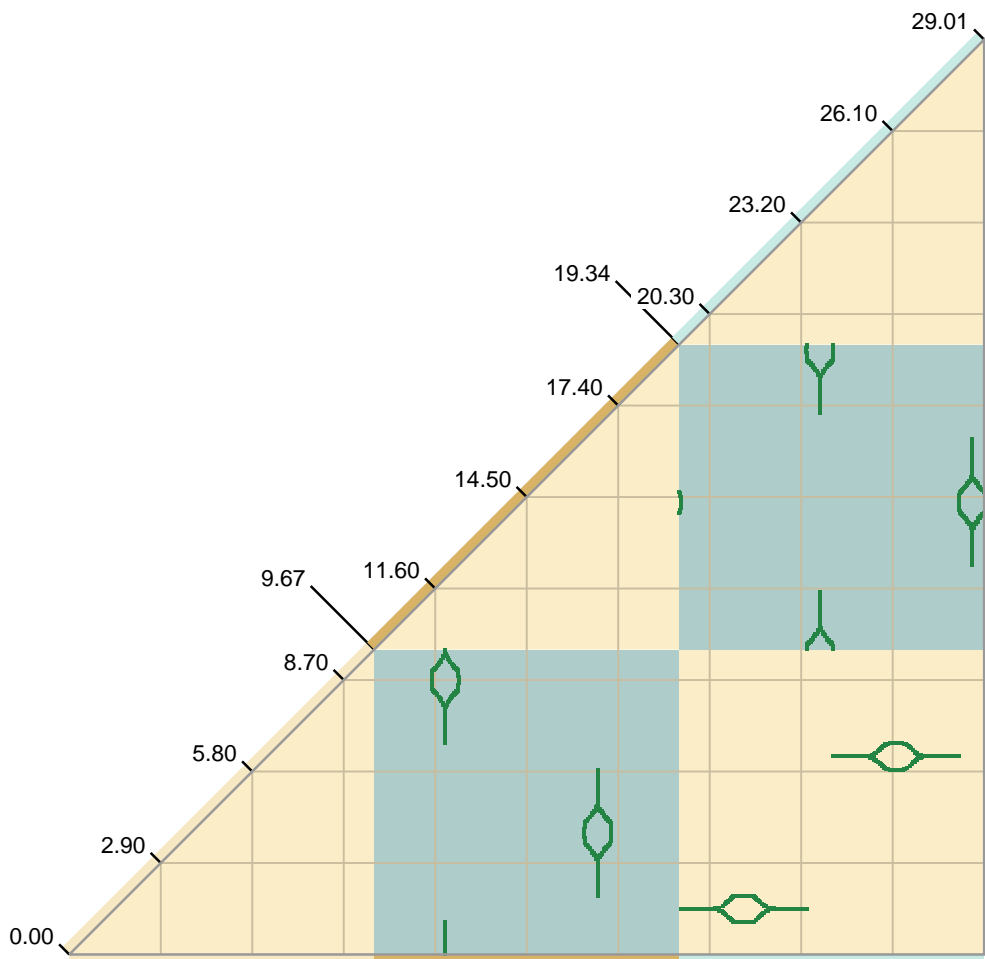


FIGURE 7. The diagonal above is labeled with arclength values along the three components of the Borromean rings link, which is numbered 6_2^3 in Rolfsen's table. Every pair $(s, t) \in \text{Strut}(\mathcal{V})$ is represented by a dark green square centered on (s, t) . As we see from the top plot, no tube around a component of the link is in contact with itself (so the three triangles near the diagonal are empty). But each of the components makes contact with the other two, as shown by the boxes plotted in the rectangles forming the remainder of the plot. We can see that the contacts break up naturally into "lantern-shaped" structures. In the bottom plot, we compare one "lantern" to the self-contact set predicted by [10], which is represented by a black line.


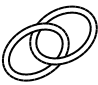


| |  |  |  |  |
|----------------------|---|---|--|---|
| Link name | Clasp | Hopf link (2_1^2) | $2_1^2 \# 2_1^2$ | Borromean rings (6_2^3) |
| Vertices | 332 | 216 | 384 | 930 |
| Rop_p bound | 4.2841 | 25.1406 | 41.7131 | 58.0192 |
| Rop bound | 4.2837 | 25.1334 | 41.7086588 | 58.0070 |
| Smooth length | 4.2629[10] | 8π [11] | $12\pi + 4$ [11] | 58.0060[10] |
| Relative error | 0.4% | 0.02% | 0.02% | 0.0017% |

TABLE 1. Numerical results from `ridgerunner` compared to the minimum ropelength values from [11] and [10]. The relative errors in the computations are quite small.

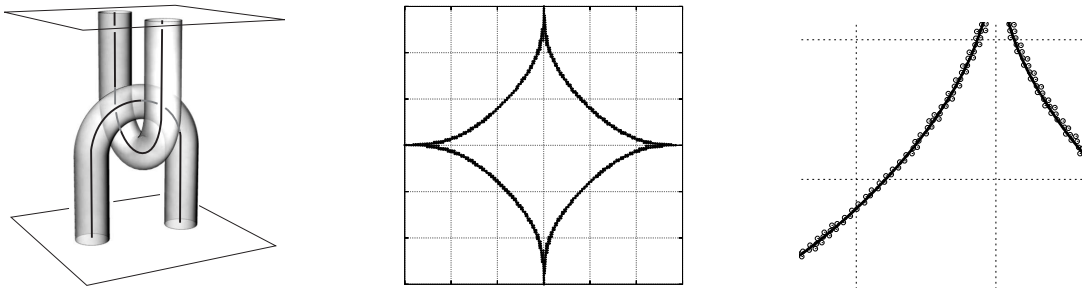


FIGURE 8. The left-hand picture shows a (loose) configuration of the “simple clasp” — a simple two-strand tangle which serves as an interesting model for the interaction between two ropes passing over each other at right angles. A ropelength-critical configuration of this tangle has been derived and studied extensively in [10] and [9]. Since this derivation included an explicit strut set, it is natural to compare `ridgerunner`’s results to this theoretical picture. This comparison is shown in the two plots center and right, which plot the positions of struts in arclength coordinates with the origin located where each curve first begins to turn. The enlarged plot (right) shows the agreement between theoretical and computational results. The data shown is from a 332 edge polygonal clasp.

a residual of 0.001 for 202 of the knots and links in our data set, proving that our knots are close to being critical for the $C\text{Thi}$ thickness. While our knots are not quite equilateral, they all satisfy the hypotheses of Corollary 2.8 and are hence also close to critical for the original Thi_p thickness. Because of this corollary, we know that both thicknesses are equal for our configurations, so we have computed and reported the Thi_p thickness and ropelength below.

We started each knot from at least five initial configurations, including the configurations from KnotPlot [49] (similar to the configurations in Rolfsen’s table), the TOROS simulated annealer [47], Gilbert’s minimized configurations from the online *Knot Atlas* [24], hand-drawn configurations from Kawauchi’s *A Survey of Knot Theory* [29], and positions generated from KnotPlot’s diagram

command. The results shown describe the lowest ropelength we achieved from any of these starting configurations.

The polygonal ropelengths for our curves appear in the column Rop_p of Tables 3-5 of Appendix A, while a plot of the ropelengths organized by crossing number appears in Figure 10.

Generating upper bounds for smooth ropelength. Our computations yielded a large set of approximate minimizers of $\text{Len}(\mathcal{V})/\text{Thi}_p(\mathcal{V})$. From these, we wanted to generate upper bounds on the minimum (smooth) ropelength of these knots and links. Rawdon has given general bounds [45, 47] on the rate at which $\text{Thi}_p \rightarrow \text{Thi}$ which we could have used for this purpose. But we were interested in small improvements in ropelength, so we used a more careful approach.

Our procedure for constructing smooth ropelength bounds from polygonal data is as follows. Beginning with \mathcal{V} , we splice circle arcs of radius $\text{MinRad}(v_i)$ into the corners at vertices v_i as shown on the left-hand side of Figure 9 to create a piecewise C^2 curve $V(s)$. The minimal radius of curvature for this curve is equal to $\text{MinRad}(\mathcal{V})$. But the self-distances of $V(s)$ may be different from those of the polygon \mathcal{V} if they involve the new circle arcs.

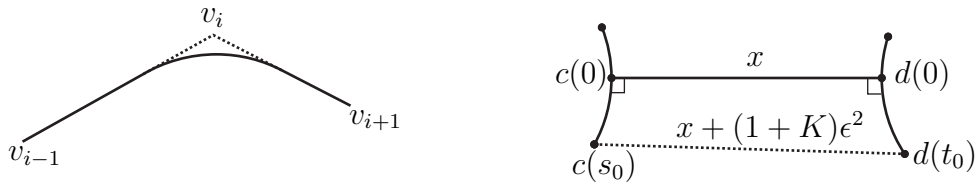


FIGURE 9. On the left, we see the curve constructed from splicing a circular arc of radius $\text{MinRad}(v_i)$ into $v_{i-1}v_iv_{i+1}$. This curve is C^1 , but not C^2 at the splice points. On the right, we see the setup for Proposition 5.1. On the left and right are arcs c and d with curvature $\leq K$ and length $\leq \epsilon$. The minimum distance x between them occurs at $c(0), d(0)$. We prove that the distance between any other pair of points $c(s_0)$ and $d(t_0)$ is bounded above by $x + (1 + K)\epsilon^2$.

We must therefore compute the self-distances of $V(s)$. This poses a problem: $\mathcal{V}(s)$ is composed of arcs of circles and line segments and Neff has shown that there is no simple formula for the distance between two arbitrary circle arcs in 3-space [38]. So we estimate the self-distances of the smooth curve $V(s)$ by taking distances between a finite number of sample points on the curve separated from one another by some ϵ . We bound the error in our computation in terms of ϵ using the following Proposition.

Proposition 5.1. *Suppose that $c(s)$ and $d(t)$ are each unit-speed piecewise C^2 arcs with curvature bounded above by K . Further, suppose that $\|c(0) - d(0)\| > 1/2$ is the minimum distance between c and d . Then for any $0 \leq s_0, t_0 \leq \epsilon$*

$$\|c(s_0) - d(t_0)\| \leq \|c(0) - d(0)\| + (1 + K)\epsilon^2.$$

Proof. Since $\|c(s) - d(t)\|$ has a local min at $(0, 0)$, we know that

$$\langle c'(0), c(0) - d(0) \rangle = 0, \quad \text{and} \quad \langle d'(0), c(0) - d(0) \rangle = 0.$$

Further, the curvature bound tells us that $\|c''\|, \|d''\| < K$. We will use these facts to estimate $\|c(s_0) - d(t_0)\|^2$. If we let $C(s_0) = \int_0^{s_0} c'(s) ds$ and $D(t_0) = \int_0^{t_0} d'(t) dt$ then we have $c(s_0) = C(s_0) + c(0)$ and $d(t_0) = D(t_0) + d(0)$, so

$$(19) \quad \|c(s_0) - d(t_0)\|^2 = \|C(s_0) - D(t_0)\|^2 - 2 \langle C(s_0) - D(t_0), c(0) - d(0) \rangle + \|c(0) - d(0)\|^2.$$

Since $c(s)$ and $d(t)$ are unit-speed curves, and $0 \leq s_0, t_0 \leq \epsilon$ we know that $\|C(s_0)\|, \|D(t_0)\| < \epsilon$ and so the first term is bounded above by $4\epsilon^2$.

The middle term is more interesting. As before, we can let $CC(s) = \int_0^s c''(x) dx$ and $DD(t) = \int_0^t d''(y) dy$, so $c'(s) = CC(s) + c'(0)$ and $d'(t) = DD(t) + d'(0)$. Since $c'(0)$ and $d'(0)$ are normal to $c(0) - d(0)$, we can then write this middle term as

$$- \langle C(s_0) - D(t_0), c(0) - d(0) \rangle = - \left\langle \int_0^{s_0} CC(s) ds - \int_0^{t_0} DD(t) dt, c(0) - d(0) \right\rangle$$

Since $\|c''\|, \|d''\| < K$, we know $\|CC(s)\| < Ks$, $\|DD(t)\| < Kt$. Thus (remembering that $s_0, t_0 < \epsilon$) the norms of the integrals on the right above are each bounded above by $K\epsilon^2/2$ and the entire dot product is bounded above by $K\epsilon^2\|c(0) - d(0)\|$.

Thus the right hand side of (19) is bounded by $\|c(0) - d(0)\|^2 + 4\epsilon^2 + 2K\epsilon^2\|c(0) - d(0)\|$. Since $1/2 < \|c(0) - d(0)\|$, $4\epsilon^2 < 2\epsilon^2\|c(0) - d(0)\|$. Using this, we see that

$$\begin{aligned} 4\epsilon^2 + 2K\epsilon^2\|c(0) - d(0)\| + \|c(0) - d(0)\|^2 &< \|c(0) - d(0)\|^2 + (2 + 2K)\epsilon^2\|c(0) - d(0)\| \\ &< \|c(0) - d(0)\|^2 + (2 + 2K)\epsilon^2\|c(0) - d(0)\| + (1 + K)^2\epsilon^4 \\ &= (\|c(0) - d(0)\| + (1 + K)\epsilon^2)^2. \end{aligned}$$

This completes the proof. □

Our code, named `roundout_rl`⁶, establishes a coarse net of points on $V(s) \times V(s) \simeq [0, 1] \times [0, 1]$ and then eliminates subsquares of this square from consideration using Proposition 5.1. The remaining squares are then subdivided and searched in turn. The process terminates once we have computed the local minima of $d(p, q)$ on the square with whatever accuracy we require.

Using `roundout_rl` in double-precision machine arithmetic we found upper bounds for the ropelengths of our 379 minimized configurations. These figures appear in column `Rop` of Tables 3-5 of Appendix A. These figures constitute the best known dataset on the lengths of tight knots and links. The data is summarized in Figure 10 and Table 2.

To test how accurate these final results are likely to be, we computed the relative residual $\|(-\nabla f)_I\|/\|-\nabla f\|$ for all these knots and links. The average residual of knots in our tabulation is about 0.00299. We have achieved residuals as low as 2.54×10^{-5} for knots and links of special interest, such as 8_{18} , 10_{123} , the trefoil, and the Borromean rings. A table of these residuals appears in Appendix A. Four knots and links in our calculation turned out to be particularly difficult for `ridgerunner`: 10_{61} , 8_{10}^3 , 8_3^4 and 9_{17}^3 .

⁶freely available as part of the `octrope` library

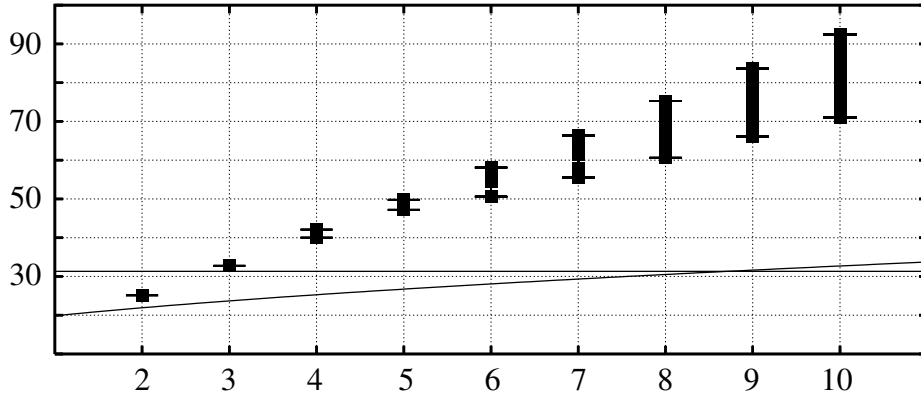


FIGURE 10. This graph shows the relationship between ropelength (y-axis) and crossing number (x-axis) for knots and links in our data set. The bottom lines show the bound of Denne et al. [17] for ropelength of a nontrivial knot (horizontal line) and Diao's bound [18] for ropelength in terms of crossing number (curve). We can see that there is a substantial overlap of ropelength values between different crossing numbers. This is reflected in Tables 6-7 of Appendix A, which show the knots in ropelength order. Table 2 shows the links of least and most ropelength for each crossing number.

| Cr | Rop | Links |
|----|--------------------|----------------------|
| 3 | 32.74 | 3_1 |
| 4 | [40.0122, 42.0887] | $4_1^2, 4_1$ |
| 5 | [47.2016, 49.7716] | $5_1, 5_1^2$ |
| 6 | [50.5539, 58.1013] | $6_3^3, 6_3^2$ |
| 7 | [55.5095, 66.3147] | $7_7^2, 7_6^2$ |
| 8 | [60.5754, 75.2592] | $8_7^3, 8_1^4$ |
| 9 | [66.0311, 83.6092] | $9_{49}^2, 9_{42}^2$ |
| 10 | [71.0739, 92.3565] | $10_{124}, 10_{123}$ |

TABLE 2. This table shows the links of smallest and largest minimum ropelength for each crossing number (according to our data). Recall that we did not minimize ten-crossing links, so it is likely that some ten-crossing link has more or less ropelength than the 10_{123} and 10_{124} knots.

Generation of tightening animations, pictures, and strut sets. We have saved the minimization runs for each of these knots and links as an animation showing the tightening knot. These animations are posted on the web at <http://www.jasoncantarella.com/movs/>.

We have also generated images of the polygonal strut sets and approximately tight configurations for each of the 379 knots and links in our data set. Space considerations prevent us from including all of this data in this paper, so they are enclosed in the associated *Atlas of Tight Links* [2]. Figure 11 shows a typical page from the *Atlas*. All of our tight knot and link data, including coordinates for

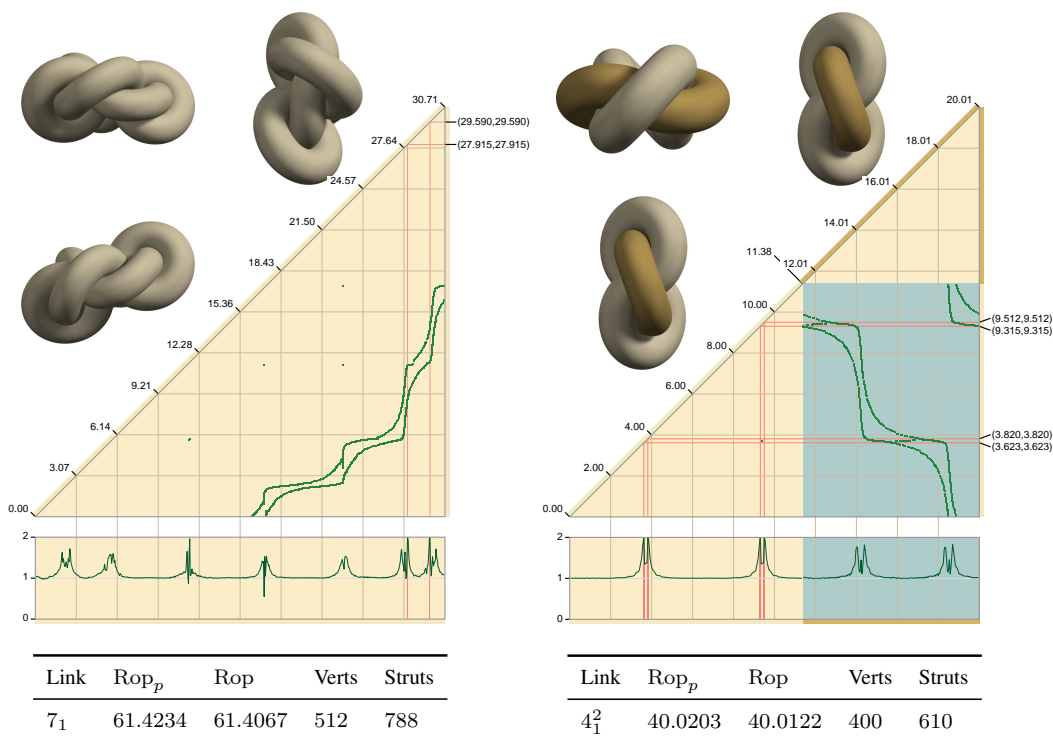


FIGURE 11. This figure shows simplified versions of two pages from the *Atlas of Tight Links* for the knot 7_1 and the link 4_1^2 . On each page, the top left pictures show three views of the link. The triangular graphic shows the struts of the link as found by `ridgerunner` plotted as points (s, t) in arclength coordinates along the link. The graph on the bottom of the page shows the curvature of the curve. The background of each plot changes color to indicate the change from one component to the next. The key along the left-to-right diagonal is given in ropelength units and color-coded with the pictures at upper left to show which component is referred to by the plot.

the tight configurations, is publicly available with the publication of this paper. We note that for technical reasons, our minimized configurations have thickness close to $1/2$ (rather than 1, as in the discussion above), and hence their maximum curvature is 2.

Discovery of symmetric tight knots. An interesting feature of the ropelength function is that minimizing ropelength seems to break any symmetry enjoyed by the original configuration of a given knot. For instance, while the minimizing configuration for the $(3, 2)$ torus knot 3_1 appears to be threefold symmetric (as expected), the minimizing configuration for the $(5, 2)$ torus knot 5_1 is not fivefold symmetric. It was therefore somewhat surprising to discover two knots in our data set, 8_{18} and 10_{123} for which the tight configurations are highly symmetric. These knots are shown in Figure 12. Their self-contact sets (which appear on pages 67 and 358 of the *Atlas*, and are reproduced in the Appendix of this paper on pages 36 and 37) are highly suggestive, resembling those of the Borromean rings (page 29), and appearing to consist of a single element repeated

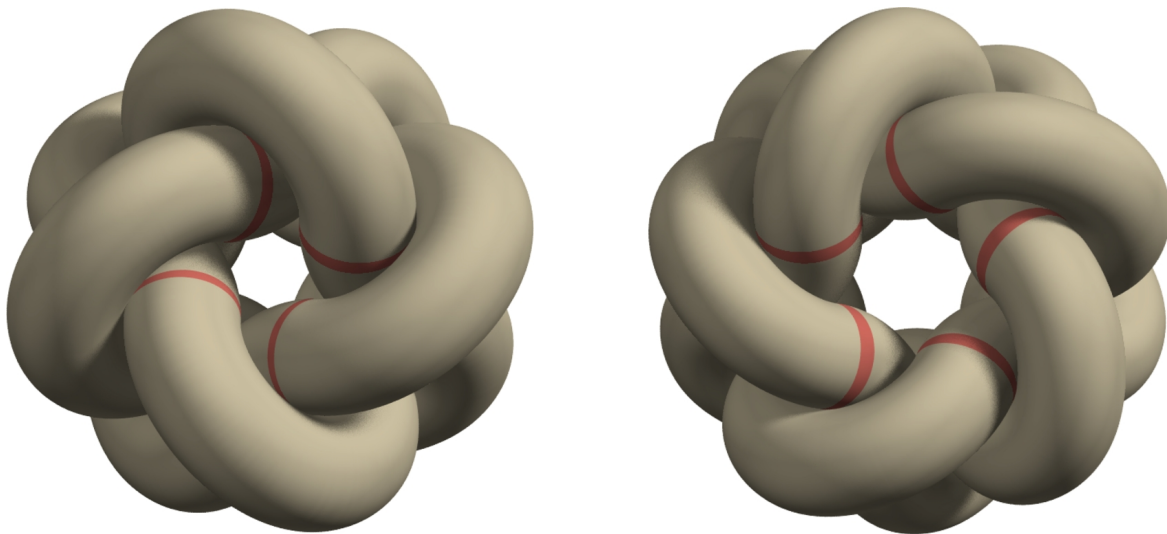


FIGURE 12. Two highly symmetric tight knots are the 8_{18} knot shown above left and the 10_{123} knot shown above right. Rounding the corners of these curves yields ropelength upper bounds of 74.9063 and 92.3565, respectively. Because their strut sets break into a particularly simple form (see pages 36 and 37), these knots may be better candidates for an explicit solution than seemingly simpler knots such as the trefoil.

several times. This feature implies that these knots may be better candidates for explicit solution than the seemingly simpler trefoil knot.

6. FUTURE DIRECTIONS

Several directions for future research suggest themselves from these experiments. First, we note that while we have given finite strut sets for several polygonal knots and observed that they are close to the 1-dimensional strut sets for the corresponding smooth tight configurations, we have not proved a theorem explaining how our polygonal strut sets converge to the strut sets of a critical polygon. We conjecture that this is part of a larger theorem which would show that if a family of polygonal ropelength critical configurations \mathcal{V}_n converge to a $C^{1,1}$ curve V then V is ropelength critical in the sense of [9], the strut sets of the \mathcal{V}_n converge in Hausdorff distance to the self-contact set of V , and the kink sets of the \mathcal{V}_n converge to the portion of V at maximum curvature.

There are several features of the tight knot data set that we have discovered that seem worthy of further investigation. Carlen, Smutny and Maddocks noted in [14] that curvature constraints seemed to be “within a rather small tolerance of being active” at several points on their numerical approximations of the tight trefoil and figure-eight knots. Baranska et al. provided numerically smoothed plots of the curvature of their approximately tight trefoil in [3] which appear to confirm this observation.

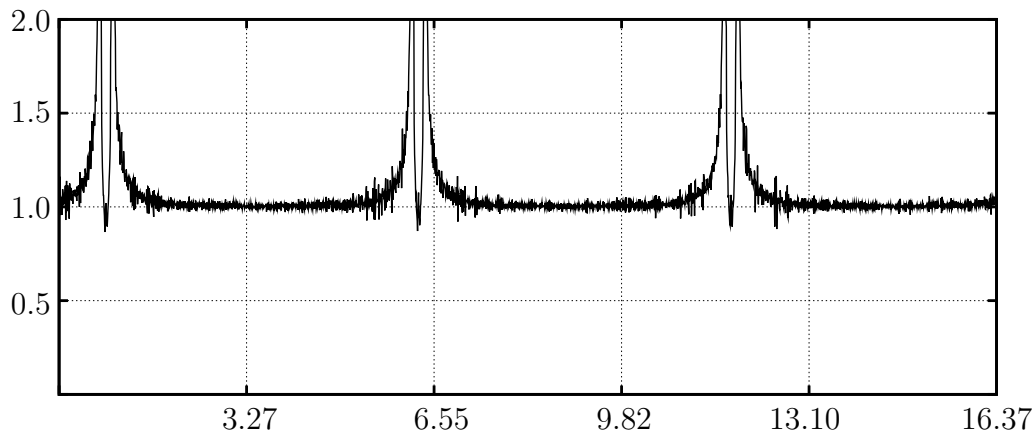


FIGURE 13. This plot shows the computed $1/\text{MinRad}$ values as a function of arclength along the polygon for a 2400 edge trefoil with thickness close to $1/2$, residual 0.0018 and polygonal ropelength 32.743663 (rounding out the corners as described above gives a smooth ropelength upper bound of 32.74352 for this configuration). The value at each vertex is plotted above with no numerical smoothing. Though there is some noise in the portions of the plot where curvature is not constrained, the six kinked regions are clearly resolved. A total of 117 vertices are involved in these regions.

We have noticed the same phenomenon in our data sets. Our computation of the curvature for the trefoil appears in Figure 13. In the *Atlas of Tight Knots*, we highlight the active curvature constraints found by `ridgerunner` as part of the minimization process by red lines on the plot of strut sets. These occur in 372 of the 379 knots and links minimized. This provides suggestive numerical evidence that kinks are rather common in tight knots. We intend to provide better evidence for this conjecture in an upcoming publication.

Several authors have proved versions of the theorem that an interval of a tight knot with curvature less than the maximum allowed and no struts must be a straight line segment [27, 50, 9, 21]. We see this phenomenon 338 times in the *Atlas*, for instance in the link 6_3^3 on page 28 of the *Atlas* (see also Figure 14), which appears to have three straight segments of length 2.1, 1.14, and 0.56. We highlight these segments in blue on the plots in the *Atlas*. These segments are almost as common as kinked regions in our data set, suggesting that they are generic features of tight configurations. Gonzalez has conjectured that every composite knot formed from joining a knot to its mirror image has a critical configuration with a pair of straight segments. We do not address this conjecture here since we only consider prime knots and links, but we do intend to compute approximately minimizing composite knots and links in a future publication.

The paper [9] (as well as [34] under very different hypotheses) shows that a pair of arcs in a tight knot coparametrized by a single family of struts and having curvature less than the maximum bound form a standard double helix. As far as we can tell, this phenomenon only occurs a few times in the *Atlas*, for instance in the 6_3^3 link on page 28, the 7_7^2 link on page 43, the 8_{19} knot on page 66, and possibly in the 8_7^3 link on page 91. It would be interesting to look for more critical configurations with double-helix sections.

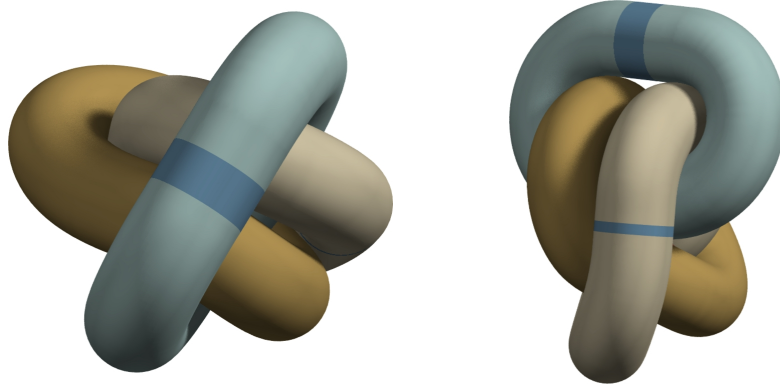


FIGURE 14. This figure shows two views of our computed tight configuration of the link 6_3^3 (ropelength upper bound 50.5539). Straight segments on the blue and white components, which occur when these components lose contact with the other components of the link, are highlighted in darker blue.

We also contemplate further improvements to our numerical knot tightening methods. The constrained gradient descent method presented in this paper is a significant improvement over simulated annealing — in practice, it has proved to be an effective minimizer for both knots and links. But this is surely not the last word in numerical ropelength minimization. Our method is a member of the class of “projected-gradient” methods introduced by Rosen and Zoutendijk in the early 1960’s [48, 54]. These algorithms are subject to a number of well-known numerical problems, such as a tendency to “wobble” when confronted with a steep-sided valley and the problem of “zigzagging”, which occurs when elements repeatedly enter and leave the strut and kink sets on successive minimization or error-correction steps. Our implementation seems to suffer from both these problems during some difficult minimizations. We have experimented with adding conjugate-gradient features to our existing code to solve these problems, but so far the results seem to yield only a slight improvement.

For these reasons, more modern methods such as sequential quadratic programming (SQP) have become the norm [23]. Codes implementing these methods require the user to specify a set of constraint functions in advance. Unfortunately, in our formulation of the constraint thickness an n -vertex polygon has $O(n^2)$ self-distance constraints and $O(n)$ turning angle or MinRad constraints. For a typical polygon with 10^3 vertices, this would mean a set of 10^6 constraints — too many to be practical. However, if we know approximately which self-distance constraints will be active in the final configuration, we can ignore constraints that we expect to be inactive, resulting in a reduced constraint set of size $O(n)$. Our approximately minimized polygons provide exactly this information. For this reason we imagine an important use of our data will be in formulating input problems for a future SQP-based knot-minimizer. Our polygons are already serving as input for the biarc-based annealer of Carlen, Smutny, and Maddocks [14].

While our data set is detailed and suggestive, solving explicitly for the structure of ropelength minimizing (smooth) knots and links is likely to require even better data. Cantarella et al. [9] have shown that a critical shape for the simple clasp formed when ropes pass over one another at right angles contains tiny straight segments of length a few thousandths of the total length of the curves.

Resolving these features will require converged runs for polygonal ropelength minimizers with tens of thousands of vertices, an ambitious goal that will keep this area of experimental mathematics active for some time to come.

7. ACKNOWLEDGEMENTS

The authors would like to mention the hard work of Sivan Toledo, whose TAUCS library made `tlsqr` and `tsnnls` possible. Our code was made much faster by Toledo's carefully written supernodal multifrontal cholesky factorization code. We are similarly indebted to Portugal, Judice and Vicente for developing the block principal pivoting algorithm. Many colleagues provided helpful conversations and insights about these and similar problems, including Joe Fu, Rob Kusner, John Sullivan, Piotr Pieranski, John Maddocks and Andrzej Stasiak. The authors would also like to acknowledge the support of the National Science Foundation through the University of Georgia VIGRE grant (DMS-00-89927), DMS-02-04826 (to Cantarella and Fu), and DMS-08-10415 (to Rawdon).

REFERENCES

- [1] Ted Ashton and Jason Cantarella. A fast octree-based algorithm for computing ropelength. In *Physical and numerical models in knot theory*, volume 36 of *Ser. Knots Everything*, pages 323–341. World Sci. Publ., Singapore, 2005.
- [2] Ted Ashton, Jason Cantarella, Michael Piatek, and Eric Rawdon. Atlas of tight links. Distributed electronically at <http://www.jasoncantarella.com/webpage/index.php?title=papers>.
- [3] J. Baranska, S. Przybyl, and P. Pieranski. Curvature and torsion of the tight closed trefoil knot. *Eur. Phys. J. B*, 66(4):547–556, 2008.
- [4] Åke Björck. *Numerical methods for least squares problems*. Society for Industrial and Applied Mathematics (SIAM), Philadelphia, PA, 1996.
- [5] Kenneth A. Brakke. The surface evolver. *Experiment. Math.*, 1(2):141–165, 1992.
- [6] Gregory Buck and Jeremy Orloff. A simple energy function for knots. *Topology Appl.*, 61(3):205–214, 1995.
- [7] Gregory Buck and Eric J. Rawdon. Role of flexibility in entanglement. *Phys. Rev. E*, 70(1):011803, 2004.
- [8] Roman V. Buny and Thomas W. Kephart. A model of glueballs. *Phys. Lett.*, B576:127–134, 2003.
- [9] Jason Cantarella, Joseph H. G. Fu, Rob Kusner, John M. Sullivan, and Nancy C. Wrinkle. On ropelength criticality. In preparation.
- [10] Jason Cantarella, Joseph H. G. Fu, Rob Kusner, John M. Sullivan, and Nancy C. Wrinkle. Criticality for the Gehring link problem. *Geom. Topol.*, 10:2055–2116 (electronic), 2006.
- [11] Jason Cantarella, Robert B. Kusner, and John M. Sullivan. On the minimum ropelength of knots and links. *Invent. Math.*, 150(2):257–286, 2002.
- [12] Jason Cantarella, Michael Piatek, and Eric Rawdon. TSNLS: A solver for large sparse least-squares problems with non-negative variables. arXiv:cs.MS/0408029.
- [13] Jason Cantarella, Michael Piatek, and Eric Rawdon. Visualizing the tightening of knots. In *VIS '05: Proceedings of the conference on Visualization '05*, pages 575–582, Washington, DC, USA, 2005. IEEE Computer Society.
- [14] M. Carlen, B. Laurie, J. H. Maddocks, and J. Smutny. Biarcs, global radius of curvature, and the computation of ideal knot shapes. In *Physical and numerical models in knot theory*, volume 36 of *Ser. Knots Everything*, pages 75–108. World Sci. Publ., Singapore, 2005.
- [15] S. S. Chern. Curves and surfaces in Euclidean space. In *Studies in Global Geometry and Analysis*, pages 16–56. Math. Assoc. Amer. (distributed by Prentice-Hall, Englewood Cliffs, N.J.), 1967.
- [16] Frank H. Clarke. Generalized gradients and applications. *Trans. Amer. Math. Soc.*, 205:247–262, 1975.

- [17] Elizabeth Denne, Yuanan Diao, and John M. Sullivan. Quadriseccants give new lower bounds for the ropelength of a knot. *Geom. Topol.*, 10:1–26 (electronic), 2006.
- [18] Yuanan Diao. The lower bounds of the lengths of thick knots. *J. Knot Theory Ramifications*, 12(1):1–16, 2003.
- [19] Manfredo P. do Carmo. *Differential geometry of curves and surfaces*. Prentice-Hall Inc., Englewood Cliffs, N.J., 1976. Translated from the Portuguese.
- [20] Akos Dobay, Jacques Dubochet, Kenneth Millett, Pierre-Edouard Sottas, and Andrzej Stasiak. Scaling behavior of random knots. *Proc. Natl. Acad. Sci. USA*, 100(10):5611–5615 (electronic), 2003.
- [21] Oguz C. Durumeric. Local structure of ideal shapes of knots. *Topology Appl.*, 154(17):3070–3089, 2007.
- [22] Herbert Federer. Curvature measures. *Trans. Amer. Math. Soc.*, 93:418–491, 1959.
- [23] R. Fletcher. *Practical methods of optimization*. Wiley-Interscience [John Wiley & Sons], New York, second edition, 2001.
- [24] Brian Gilbert. Ideal knot and link data. http://katlas.math.toronto.edu/wiki/Ideal_knots.
- [25] O. Gonzalez and R. de la Llave. Existence of ideal knots. *J. Knot Theory Ramifications*, 12(1):123–133, 2003.
- [26] O. Gonzalez, J. H. Maddocks, F. Schuricht, and H. von der Mosel. Global curvature and self-contact of nonlinearly elastic curves and rods. *Calc. Var. Partial Differential Equations*, 14(1):29–68, 2002.
- [27] Oscar Gonzalez and John H. Maddocks. Global curvature, thickness, and the ideal shapes of knots. *Proc. Natl. Acad. Sci. USA*, 96(9):4769–4773 (electronic), 1999.
- [28] Vsevolod Katritch, Jan Bednar, Didier Michoud, Robert G. Scharein, Jacques Dubochet, and Andrzej Stasiak. Geometry and physics of knots. *Nature*, 384(6605):142–145, 1996.
- [29] Akio Kawachi. *A survey of knot theory*. Birkhäuser Verlag, Basel, 1996. Translated and revised from the 1990 Japanese original by the author.
- [30] Otto Krötenheerdt and Sigrid Veit. Zur Theorie massiver Knoten. *Wiss. Beitr. Martin-Luther-Univ. Halle-Wittenberg Reihe M Math.*, 7:61–74, 1976.
- [31] Otto Krötenheerdt and Sigrid Veit. On the theory of solid knots [mr0436119]. In *Physical and numerical models in knot theory*, volume 36 of *Ser. Knots Everything*, pages 1–18. World Sci. Publ., Singapore, 2005. Translated from the German and with notes by Ted Ashton.
- [32] Ben Laurie. Annealing ideal knots and links: methods and pitfalls. In *Ideal knots*, volume 19 of *Ser. Knots Everything*, pages 42–51. World Sci. Publishing, River Edge, NJ, 1998.
- [33] R. A. Litherland, J. Simon, O. Durumeric, and E. Rawdon. Thickness of knots. *Topology Appl.*, 91(3):233–244, 1999.
- [34] John H. Maddocks and Joseph B. Keller. Ropes in equilibrium. *SIAM J. Appl. Math.*, 47(6):1185–1200, 1987.
- [35] O. L. Mangasarian and S. Fromovitz. The Fritz John necessary optimality conditions in the presence of equality and inequality constraints. *J. Math. Anal. Appl.*, 17:37–47, 1967.
- [36] Cristian Micheletti, Jaynath Banavar, Amos Maritan, and F. Seno. Protein structures and optimal folding from a geometric variational principle. *Physical Review Letters*, 82:3372–3375, 1999.
- [37] Alexander Nabutovsky. Non-recursive functions, knots “with thick ropes”, and self-clenching “thick” hyperspheres. *Comm. Pure Appl. Math.*, 48(4):381–428, 1995.
- [38] C. A. Neff. Finding the distance between two circles in three-dimensional space. *IBM J. Res. Develop.*, 34(5):770–775, 1990.
- [39] Christopher C. Paige and Michael A. Saunders. LSQR: An algorithm for sparse linear equations and sparse least squares. *ACM Trans. Math. Softw.*, 8(1):43–71, 1982.
- [40] Michael J. Panik. *Fundamentals of Convex Analysis: Duality, Separation, Representation, and Resolution*, volume 24 of *Theory and Decision Library, Series B: Mathematical and Statistical Methods*. Kluwer Academic Publishers, 1993.
- [41] Piotr Pierański. In search of ideal knots. In *Ideal knots*, volume 19 of *Ser. Knots Everything*, pages 20–41. World Sci. Publishing, River Edge, NJ, 1998.
- [42] Piotr Pieranski, Sandor Kasas, Giovanni Dietler, Jacques Dubochet, and Andrzej Stasiak. Localization of breakage points in knotted strings. *New Journal of Physics*, 3:10, 2001.
- [43] Luís F. Portugal, Joaquim J. Júdice, and Luís N. Vicente. A comparison of block pivoting and interior-point algorithms for linear least squares problems with nonnegative variables. *Math. Comp.*, 63(208):625–643, 1994.
- [44] Eric Rawdon. *The Thickness of Polygonal Knots*. PhD thesis, The University of Iowa, 1997.
- [45] Eric J. Rawdon. Approximating the thickness of a knot. In *Ideal knots*, volume 19 of *Ser. Knots Everything*, pages 143–150. World Sci. Publishing, River Edge, NJ, 1998.

- [46] Eric J. Rawdon. Approximating smooth thickness. *J. Knot Theory Ramifications*, 9(1):113–145, 2000.
- [47] Eric J. Rawdon. Can computers discover ideal knots? *Experiment. Math.*, 12(3):287–302, 2003.
- [48] J. B. Rosen. The gradient projection method for nonlinear programming. II. Nonlinear constraints. *J. Soc. Indust. Appl. Math.*, 9:514–532, 1961.
- [49] Robert G. Scharein. KnotPlot. <http://www.knotplot.com>. Program for drawing, visualizing, manipulating, and energy minimizing knots.
- [50] Friedemann Schuricht and Heiko von der Mosel. Characterization of ideal knots. *Calc. Var. Partial Differential Equations*, 19(3):281–305, 2004.
- [51] Josef Stoer and Christoph Witzgall. *Convexity and optimization in finite dimensions. I.* Die Grundlehren der mathematischen Wissenschaften, Band 163. Springer-Verlag, New York, 1970.
- [52] John M. Sullivan. Approximating ropelength by energy functions. In *Physical knots: knotting, linking, and folding geometric objects in \mathbb{R}^3 (Las Vegas, NV, 2001)*, volume 304 of *Contemp. Math.*, pages 181–186. Amer. Math. Soc., Providence, RI, 2002.
- [53] Sivan Toledo, Vladimir Rotkin, and Doron Chen. TAUCS: A library of sparse linear solvers, 2003. <http://www.tau.ac.il/~stoledo/taucs/>.
- [54] G. Zoutendijk. Maximizing a function in a convex region. *J. Roy. Statist. Soc. Ser. B*, 21:338–355, 1959.

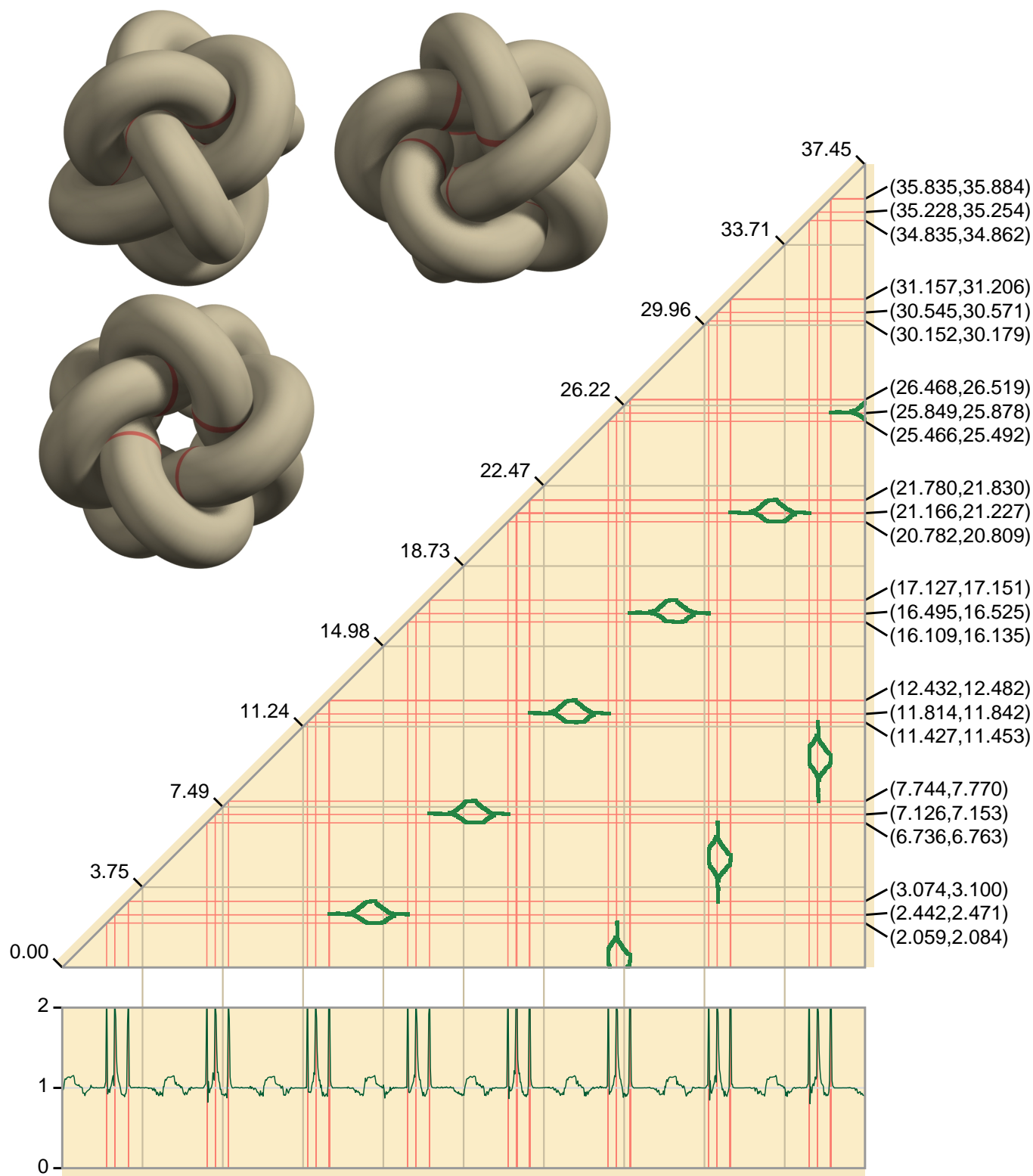
APPENDIX A. ROPELENGTH DATA

The pages that follow contain three sets of tables of ropelength data. The first set, Tables 3–5 on pages 38–40, show the polygonal ropelength (Rop_p) and ropelength upper bounds (Rop) that we have obtained for each of the knot types that we have considered. The knots and links are organized according to their position in Rolfsen’s table, with the link X_z^y being the z -th example of a prime X -crossing link of y components in the table. We have identified the two “Perko pair” knots 10_{161} and 10_{162} and renumbered the subsequent knots accordingly, so there are only 165 ten-crossing knots in our results.

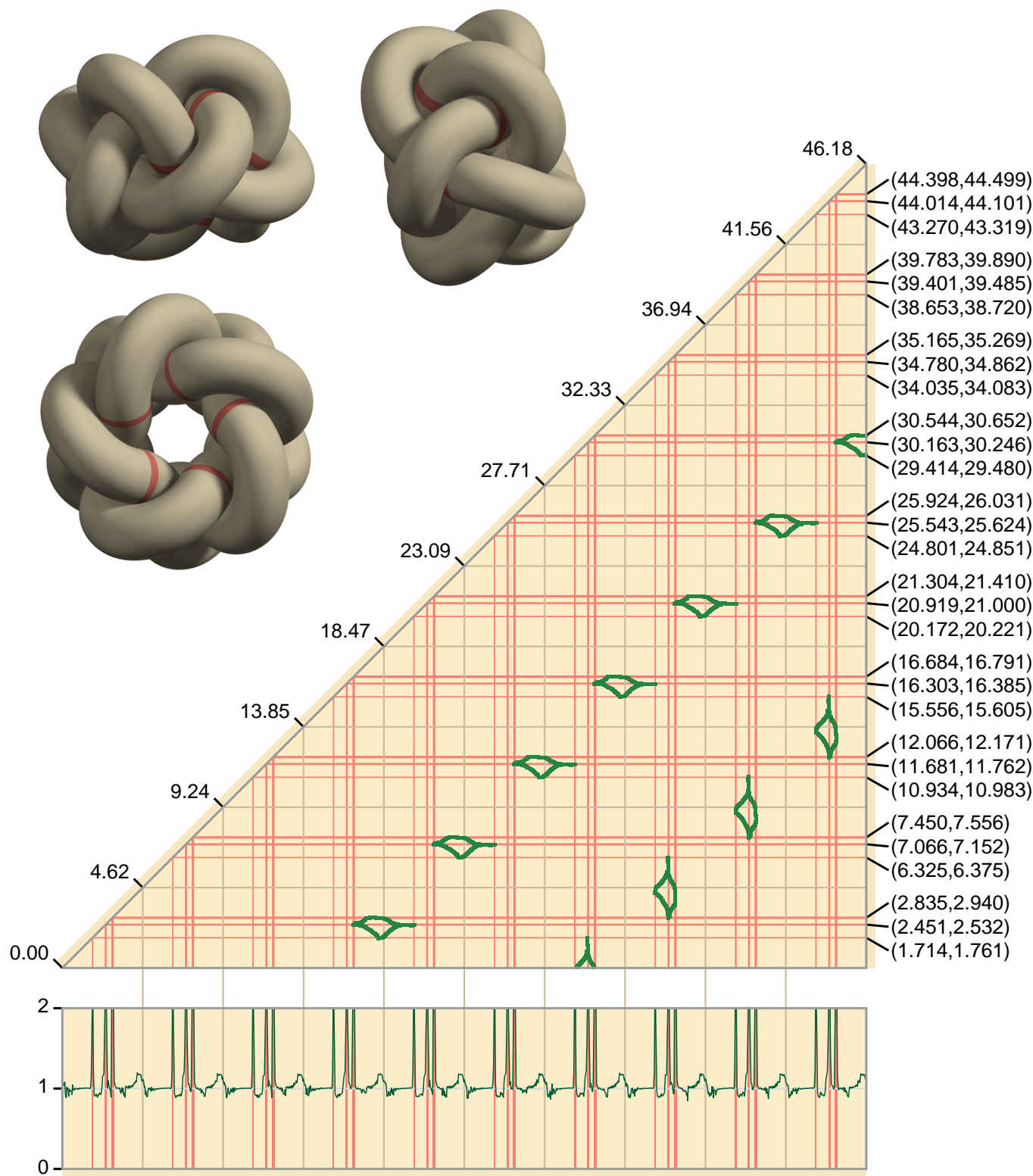
The second set, Tables 6 and 7 on pages 41–42, show the same knot and link types ordered by ropelength upper bound. These tables are to be read down each column from the top left to the bottom right. We can see that this order is quite different from the one in Rolfsen’s table with (for instance) the 2-component link 7_7^2 occurring before any 6 or 7 crossing knot and the 10_{124} knot occurring before many 8 and 9 crossing links.

The third set of tables, Tables 8–10 on pages 43–45 give the residual of each of our computed configurations. The low residuals show that they are close to critical in the sense of Theorem 2.18. We include this data as measure of the relative quality of each of our minimized configurations.

On pages 36–37 are reproductions of the pages from the *Atlas of Tight Knots* for the approximately tight 8_{18} and 10_{123} knots. On the top left of each page are three views of the tight configurations, with kinked regions highlighted in red. On the top right is a plot of the self-contact map of the configuration. Each of these plots consists of a triangular region with the hypotenuse labeled with arclength values on the knot. A green box is plotted at (s, t) on the plot if there is a strut connecting $L(s)$ and $L(t)$. Below the graph appears a plot of $1/\text{MinRad}$ for the polygon (to the same scale). Kinked regions of maximum curvature are plotted in red on the graph. Each such region has a key on the right-hand side of the plot showing the arclength positions of the start and end of the kink (in order to give a sense of the relative scale of the kinked region). At the bottom of the page is a line of data giving the polygonal ropelength Rop_p (as measured by `octrope`), ropelength upper bound Rop (from `roundout_rl`), filename, number of vertices and struts, maximum and minimum curvature values and number of kinked regions. The last entry shows the total arclength of straight regions in the curves (0 for these two knots, but nonzero for many knots and links in the *Atlas*).



| Link | Rop_p | Rop | Filename | Verts | Struts | κ range | Kink | Straight |
|----------|---------|---------|----------------------|-------|--------|---------------------|------|----------|
| 8_{18} | 74.9114 | 74.9063 | kl_8_18_hrbanff.vect | 1199 | 5591 | [0.802748, 2.00005] | 24 | |



| Link | Rop_p | Rop | Filename | Verts | Struts | κ range | Kink | Straight |
|------------|---------|---------|----------------------------|-------|--------|--------------------|------|----------|
| 10_{123} | 92.3646 | 92.3565 | kl_10_123_handcrafted.vect | 1498 | 7189 | [0.84917, 2.00008] | 30 | |

TABLE 3. Part 1 of Ropelengths of Tight Knots and Links by Knot Type

| Link | Rop_p | Rop | Link | Rop_p | Rop | Link | Rop_p | Rop |
|---------|---------|---------|------------|---------|---------|------------|---------|---------|
| 2_1^2 | 25.1415 | 25.1334 | 8_2 | 71.4141 | 71.3985 | 8_8^3 | 65.0195 | 65.0042 |
| 3_1 | 32.7437 | 32.7436 | 8_3 | 71.1736 | 71.1575 | 8_9^3 | 66.7076 | 66.6936 |
| 4_1 | 42.0971 | 42.0887 | 8_4 | 71.4872 | 71.4704 | 8_{10}^3 | 68.4580 | 68.4503 |
| 4_1^2 | 40.0203 | 40.0122 | 8_5 | 72.1519 | 72.1344 | 8_1^4 | 75.2748 | 75.2592 |
| 5_1 | 47.2149 | 47.2016 | 8_6 | 72.4903 | 72.4725 | 8_2^4 | 67.4087 | 67.3937 |
| 5_2 | 49.4820 | 49.4701 | 8_7 | 72.2292 | 72.2137 | 8_3^4 | 66.2969 | 66.2865 |
| 5_1^2 | 49.7864 | 49.7716 | 8_8 | 72.7438 | 72.7241 | 9_1 | 75.5663 | 75.5461 |
| 6_1 | 56.7178 | 56.7058 | 8_9 | 72.4568 | 72.4399 | 9_2 | 78.1231 | 78.1066 |
| 6_2 | 57.0381 | 57.0235 | 8_{10} | 72.9580 | 72.9379 | 9_3 | 78.2040 | 78.1892 |
| 6_3 | 57.8531 | 57.8392 | 8_{11} | 72.9110 | 72.8966 | 9_4 | 78.2793 | 78.2665 |
| 6_1^2 | 54.3919 | 54.3768 | 8_{12} | 73.9707 | 73.9518 | 9_5 | 78.6615 | 78.6447 |
| 6_2^2 | 56.7087 | 56.7000 | 8_{13} | 72.8194 | 72.8000 | 9_6 | 79.5802 | 79.5597 |
| 6_3^2 | 58.1142 | 58.1013 | 8_{14} | 73.7784 | 73.7612 | 9_7 | 79.6924 | 79.6731 |
| 6_1^3 | 57.8286 | 57.8141 | 8_{15} | 73.9076 | 73.8977 | 9_8 | 80.0276 | 80.0080 |
| 6_2^3 | 58.0112 | 58.0070 | 8_{16} | 73.5207 | 73.5054 | 9_9 | 79.8965 | 79.8778 |
| 6_3^3 | 50.5602 | 50.5539 | 8_{17} | 74.5075 | 74.4912 | 9_{10} | 79.8009 | 79.7855 |
| 7_1 | 61.4234 | 61.4067 | 8_{18} | 74.9114 | 74.9063 | 9_{11} | 80.1355 | 80.1180 |
| 7_2 | 63.8684 | 63.8556 | 8_{19} | 60.9970 | 60.9858 | 9_{12} | 80.0997 | 80.0834 |
| 7_3 | 63.9430 | 63.9285 | 8_{20} | 63.1066 | 63.0929 | 9_{13} | 80.2657 | 80.2498 |
| 7_4 | 64.2836 | 64.2687 | 8_{21} | 65.5387 | 65.5248 | 9_{14} | 80.0193 | 80.0001 |
| 7_5 | 65.2705 | 65.2560 | 8_1^2 | 68.4208 | 68.4045 | 9_{15} | 80.8941 | 80.8725 |
| 7_6 | 65.7068 | 65.6924 | 8_2^2 | 71.0493 | 71.0311 | 9_{16} | 80.1334 | 80.1143 |
| 7_7 | 65.6235 | 65.6086 | 8_3^2 | 72.7292 | 72.7133 | 9_{17} | 80.4718 | 80.4530 |
| 7_1^2 | 64.2484 | 64.2345 | 8_4^2 | 72.5995 | 72.5855 | 9_{18} | 81.5816 | 81.5673 |
| 7_2^2 | 65.0363 | 65.0204 | 8_5^2 | 73.9503 | 73.9331 | 9_{19} | 80.9196 | 80.9004 |
| 7_3^2 | 65.3414 | 65.3257 | 8_6^2 | 73.2133 | 73.1955 | 9_{20} | 80.2421 | 80.2219 |
| 7_4^2 | 65.0759 | 65.0602 | 8_7^2 | 74.3917 | 74.3752 | 9_{21} | 81.1083 | 81.0920 |
| 7_5^2 | 66.2068 | 66.1915 | 8_8^2 | 73.7714 | 73.7540 | 9_{22} | 81.0587 | 81.0390 |
| 7_6^2 | 66.3281 | 66.3147 | 8_9^2 | 73.2196 | 73.2038 | 9_{23} | 81.2922 | 81.2733 |
| 7_7^2 | 55.5177 | 55.5095 | 8_{10}^2 | 73.6729 | 73.6548 | 9_{24} | 80.9626 | 80.9451 |
| 7_8^2 | 57.7714 | 57.7631 | 8_{11}^2 | 72.9786 | 72.9608 | 9_{25} | 81.1348 | 81.1198 |
| 7_1^3 | 65.8157 | 65.8062 | 8_{12}^2 | 73.8018 | 73.7846 | 9_{26} | 80.9241 | 80.9053 |
| 8_1 | 70.9833 | 70.9669 | 8_{13}^2 | 74.1522 | 74.1369 | 9_{27} | 81.1838 | 81.1813 |
| 8_2 | 71.4141 | 71.3985 | 8_{14}^2 | 73.6878 | 73.6695 | 9_{28} | 81.0878 | 81.1352 |
| | | | 8_{15}^2 | 64.3105 | 64.2996 | 9_{29} | 81.2019 | 81.1821 |
| | | | 8_{16}^2 | 66.8148 | 66.8046 | 9_{30} | 81.4811 | 81.4883 |
| | | | 8_1^3 | 72.2765 | 72.2603 | 9_{31} | 81.6751 | 81.6581 |
| | | | 8_2^3 | 72.9357 | 72.9181 | 9_{32} | 81.5343 | 81.5175 |
| | | | 8_3^3 | 74.8824 | 74.8656 | 9_{33} | 82.7691 | 82.7541 |
| | | | 8_4^3 | 75.0026 | 74.9866 | 9_{34} | 82.1884 | 82.1706 |
| | | | 8_5^3 | 73.4072 | 73.3932 | 9_{35} | 79.2390 | 79.2165 |
| | | | 8_6^3 | 74.7320 | 74.7159 | 9_{36} | 80.2275 | 80.2064 |
| | | | 8_7^3 | 60.5897 | 60.5754 | 9_{37} | 81.1744 | 81.1674 |
| | | | 8_8^3 | 65.0195 | 65.0042 | 9_{38} | 81.7858 | 81.7697 |

TABLE 4. Part 2 of Ropelengths of Tight Knots and Links by Knot Type

| Link | Rop_p | Rop | Link | Rop_p | Rop | Link | Rop_p | Rop |
|------------------------------|---------|---------|------------------------------|---------|---------|------------------------------|---------|---------|
| 9 ₃₈ | 81.7858 | 81.7697 | 9 ₃₃ ² | 82.1790 | 82.1612 | 9 ₁₆ ³ | 75.0113 | 75.0003 |
| 9 ₃₉ | 81.8439 | 81.8264 | 9 ₃₄ ² | 81.8490 | 81.8320 | 9 ₁₇ ³ | 74.1280 | 74.1159 |
| 9 ₄₀ | 81.6652 | 81.6474 | 9 ₃₅ ² | 81.2508 | 81.2318 | 9 ₁₈ ³ | 72.4529 | 72.4382 |
| 9 ₄₁ | 81.3687 | 81.3540 | 9 ₃₆ ² | 80.7066 | 80.6866 | 9 ₁₉ ³ | 72.6412 | 72.6275 |
| 9 ₄₂ | 69.4867 | 69.4756 | 9 ₃₇ ² | 81.9102 | 81.8927 | 9 ₂₀ ³ | 75.9995 | 75.9845 |
| 9 ₄₃ | 71.5050 | 71.4901 | 9 ₃₈ ² | 82.6750 | 82.6561 | 9 ₂₁ ³ | 74.8967 | 74.8908 |
| 9 ₄₄ | 71.5587 | 71.5427 | 9 ₃₉ ² | 81.8972 | 81.8758 | | | |
| 9 ₄₅ | 74.0861 | 74.0761 | 9 ₄₀ ² | 81.9680 | 81.9460 | 9 ₁ ⁴ | 81.6096 | 81.5927 |
| 9 ₄₆ | 68.6330 | 68.6169 | 9 ₄₁ ² | 83.6038 | 83.5878 | | | |
| 9 ₄₇ | 74.8935 | 74.8785 | 9 ₄₂ ² | 83.6304 | 83.6092 | 10 ₁ | 85.1146 | 85.0947 |
| 9 ₄₈ | 74.0317 | 74.0228 | 9 ₄₃ ² | 66.2549 | 66.2398 | 10 ₂ | 85.6050 | 85.5850 |
| 9 ₄₉ | 73.9403 | 73.9286 | 9 ₄₄ ² | 72.2072 | 72.1896 | 10 ₃ | 85.4483 | 85.4278 |
| | | | 9 ₄₅ ² | 71.0815 | 71.0726 | 10 ₄ | 85.8181 | 85.7974 |
| 9 ₁ ² | 78.6049 | 78.5862 | 9 ₄₆ ² | 73.8347 | 73.8215 | 10 ₅ | 86.4952 | 86.4741 |
| 9 ₂ ² | 79.5287 | 79.5152 | 9 ₄₇ ² | 69.9130 | 69.8983 | 10 ₆ | 86.8353 | 86.8125 |
| 9 ₃ ² | 79.9495 | 79.9312 | 9 ₄₈ ² | 73.6563 | 73.6426 | 10 ₇ | 87.2979 | 87.2775 |
| 9 ₄ ² | 78.6961 | 78.6764 | 9 ₄₉ ² | 66.0444 | 66.0311 | 10 ₈ | 85.8620 | 85.8428 |
| 9 ₅ ² | 79.6569 | 79.6384 | 9 ₅₀ ² | 69.3353 | 69.3284 | 10 ₉ | 86.8410 | 86.8222 |
| 9 ₆ ² | 80.1200 | 80.1017 | 9 ₅₁ ² | 70.5455 | 70.5299 | 10 ₁₀ | 87.2060 | 87.1870 |
| 9 ₇ ² | 81.1437 | 81.1261 | 9 ₅₂ ² | 72.8271 | 72.8106 | 10 ₁₁ | 86.9848 | 86.9630 |
| 9 ₈ ² | 80.9964 | 80.9766 | 9 ₅₃ ² | 68.0154 | 68.0082 | 10 ₁₂ | 87.1055 | 87.0824 |
| 9 ₉ ² | 80.3174 | 80.2999 | 9 ₅₄ ² | 71.0240 | 71.0089 | 10 ₁₃ | 88.9148 | 88.8989 |
| 9 ₁₀ ² | 80.3218 | 80.3036 | 9 ₅₅ ² | 73.8129 | 73.7998 | 10 ₁₄ | 88.3232 | 88.3023 |
| 9 ₁₁ ² | 82.0329 | 82.0140 | 9 ₅₆ ² | 72.9013 | 72.8833 | 10 ₁₅ | 87.4787 | 87.4606 |
| 9 ₁₂ ² | 81.9602 | 81.9414 | 9 ₅₇ ² | 72.2115 | 72.1922 | 10 ₁₆ | 87.4946 | 87.4684 |
| 9 ₁₃ ² | 79.3468 | 79.3280 | 9 ₅₈ ² | 74.1685 | 74.1499 | 10 ₁₇ | 87.0473 | 87.0277 |
| 9 ₁₄ ² | 80.7276 | 80.7104 | 9 ₅₉ ² | 72.3285 | 72.3130 | 10 ₁₈ | 88.4257 | 88.4092 |
| 9 ₁₅ ² | 80.5659 | 80.5458 | 9 ₆₀ ² | 73.5589 | 73.5442 | 10 ₁₉ | 87.5311 | 87.5099 |
| 9 ₁₆ ² | 81.3758 | 81.3565 | 9 ₆₁ ² | 69.3751 | 69.3636 | 10 ₂₀ | 86.8731 | 86.8514 |
| 9 ₁₇ ² | 80.3223 | 80.3022 | | | | 10 ₂₁ | 87.0497 | 87.0343 |
| 9 ₁₈ ² | 81.7563 | 81.7461 | 9 ₁ ³ | 81.1522 | 81.1333 | 10 ₂₂ | 87.2417 | 87.2182 |
| 9 ₁₉ ² | 79.4706 | 79.4491 | 9 ₂ ³ | 81.7304 | 81.7190 | 10 ₂₃ | 88.7048 | 88.6901 |
| 9 ₂₀ ² | 80.1357 | 80.1147 | 9 ₃ ³ | 82.2498 | 82.2346 | 10 ₂₄ | 88.4160 | 88.3963 |
| 9 ₂₁ ² | 80.6010 | 80.5824 | 9 ₄ ³ | 82.5202 | 82.5029 | 10 ₂₅ | 88.7767 | 88.7587 |
| 9 ₂₂ ² | 81.0964 | 81.0794 | 9 ₅ ³ | 80.2664 | 80.2456 | 10 ₂₆ | 88.4564 | 88.4328 |
| 9 ₂₃ ² | 80.2592 | 80.2379 | 9 ₆ ³ | 80.9434 | 80.9258 | 10 ₂₇ | 89.8944 | 89.8795 |
| 9 ₂₄ ² | 81.7913 | 81.7691 | 9 ₇ ³ | 82.0540 | 82.0378 | 10 ₂₈ | 87.5276 | 87.5061 |
| 9 ₂₅ ² | 81.7810 | 81.7630 | 9 ₈ ³ | 81.1278 | 81.1107 | 10 ₂₉ | 89.2410 | 89.2238 |
| 9 ₂₆ ² | 82.1031 | 82.0859 | 9 ₉ ³ | 81.5469 | 81.5295 | 10 ₃₀ | 88.3731 | 88.3558 |
| 9 ₂₇ ² | 81.0288 | 81.0141 | 9 ₁₀ ³ | 82.3146 | 82.2964 | 10 ₃₁ | 88.2624 | 88.2401 |
| 9 ₂₈ ² | 81.3352 | 81.3222 | 9 ₁₁ ³ | 82.0023 | 81.9867 | 10 ₃₂ | 88.6809 | 88.6597 |
| 9 ₂₉ ² | 82.1606 | 82.1445 | 9 ₁₂ ³ | 82.4811 | 82.4608 | 10 ₃₃ | 88.2952 | 88.2744 |
| 9 ₃₀ ² | 82.2155 | 82.1987 | 9 ₁₃ ³ | 72.2098 | 72.2009 | 10 ₃₄ | 87.0322 | 87.0101 |
| 9 ₃₁ ² | 80.5732 | 80.5561 | 9 ₁₄ ³ | 74.4319 | 74.4205 | 10 ₃₅ | 88.0891 | 88.0697 |
| 9 ₃₂ ² | 81.4151 | 81.3990 | 9 ₁₅ ³ | 74.2998 | 74.2810 | 10 ₃₆ | 88.0424 | 88.0233 |
| 9 ₃₃ ² | 82.1790 | 82.1612 | 9 ₁₆ ³ | 75.0113 | 75.0003 | 10 ₃₇ | 88.1319 | 88.1153 |

TABLE 5. Part 3 of Ropelengths of Tight Knots and Links by Knot Type

| Link | Rop_p | Rop | Link | Rop_p | Rop | Link | Rop_p | Rop |
|------------------|---------|---------|-------------------|---------|---------|-------------------|---------|---------|
| 10 ₃₇ | 88.1319 | 88.1153 | 10 ₈₀ | 89.1669 | 89.1556 | 10 ₁₂₃ | 92.3646 | 92.3565 |
| 10 ₃₈ | 88.3478 | 88.3257 | 10 ₈₁ | 90.0181 | 90.0007 | 10 ₁₂₄ | 71.0894 | 71.0739 |
| 10 ₃₉ | 88.3562 | 88.3323 | 10 ₈₂ | 88.7011 | 88.6801 | 10 ₁₂₅ | 74.9907 | 74.9778 |
| 10 ₄₀ | 89.2659 | 89.2464 | 10 ₈₃ | 89.5544 | 89.5314 | 10 ₁₂₆ | 77.6202 | 77.6026 |
| 10 ₄₁ | 89.0725 | 89.0553 | 10 ₈₄ | 89.6518 | 89.6788 | 10 ₁₂₇ | 80.0235 | 80.0124 |
| 10 ₄₂ | 89.9013 | 89.8857 | 10 ₈₅ | 87.8403 | 87.8164 | 10 ₁₂₈ | 76.4187 | 76.4026 |
| 10 ₄₃ | 89.3512 | 89.3366 | 10 ₈₆ | 88.7050 | 88.6851 | 10 ₁₂₉ | 78.5739 | 78.5553 |
| 10 ₄₄ | 88.8714 | 88.8515 | 10 ₈₇ | 89.1363 | 89.1173 | 10 ₁₃₀ | 78.8499 | 78.8356 |
| 10 ₄₅ | 89.4836 | 89.4621 | 10 ₈₈ | 89.5638 | 89.5461 | 10 ₁₃₁ | 81.2871 | 81.2678 |
| 10 ₄₆ | 86.4718 | 86.4487 | 10 ₈₉ | 89.4343 | 89.4178 | 10 ₁₃₂ | 74.7441 | 74.7330 |
| 10 ₄₇ | 87.3043 | 87.2821 | 10 ₉₀ | 88.9330 | 88.9115 | 10 ₁₃₃ | 77.1813 | 77.1631 |
| 10 ₄₈ | 87.3814 | 87.3643 | 10 ₉₁ | 88.9611 | 88.9435 | 10 ₁₃₄ | 78.6521 | 78.6377 |
| 10 ₄₉ | 88.2914 | 88.2705 | 10 ₉₂ | 89.6200 | 89.6011 | 10 ₁₃₅ | 81.2305 | 81.2157 |
| 10 ₅₀ | 87.3876 | 87.3716 | 10 ₉₃ | 88.3962 | 88.3773 | 10 ₁₃₆ | 78.0398 | 78.0276 |
| 10 ₅₁ | 88.3209 | 88.3002 | 10 ₉₄ | 88.8514 | 88.8306 | 10 ₁₃₇ | 79.6352 | 79.6185 |
| 10 ₅₂ | 88.0719 | 88.0565 | 10 ₉₅ | 90.0056 | 89.9848 | 10 ₁₃₈ | 82.5504 | 82.5320 |
| 10 ₅₃ | 88.8361 | 88.8180 | 10 ₉₆ | 89.5493 | 89.5284 | 10 ₁₃₉ | 72.9001 | 72.8944 |
| 10 ₅₄ | 87.5336 | 87.5127 | 10 ₉₇ | 89.4340 | 89.4163 | 10 ₁₄₀ | 73.8610 | 73.8477 |
| 10 ₅₅ | 88.3760 | 88.3699 | 10 ₉₈ | 89.7172 | 89.6969 | 10 ₁₄₁ | 76.9687 | 76.9543 |
| 10 ₅₆ | 89.0160 | 88.9973 | 10 ₉₉ | 88.8926 | 88.8734 | 10 ₁₄₂ | 75.8951 | 75.8754 |
| 10 ₅₇ | 89.6126 | 89.5946 | 10 ₁₀₀ | 88.7124 | 88.6927 | 10 ₁₄₃ | 78.2422 | 78.2307 |
| 10 ₅₈ | 88.9623 | 88.9445 | 10 ₁₀₁ | 89.7344 | 89.7210 | 10 ₁₄₄ | 81.4378 | 81.4275 |
| 10 ₅₉ | 89.2228 | 89.2090 | 10 ₁₀₂ | 88.7969 | 88.7734 | 10 ₁₄₅ | 75.9194 | 75.9076 |
| 10 ₆₀ | 89.3397 | 89.3190 | 10 ₁₀₃ | 88.7971 | 88.7914 | 10 ₁₄₆ | 79.7416 | 79.7322 |
| 10 ₆₁ | 86.4755 | 86.4561 | 10 ₁₀₄ | 91.7476 | 91.7280 | 10 ₁₄₇ | 79.1666 | 79.1571 |
| 10 ₆₂ | 87.5318 | 87.5071 | 10 ₁₀₅ | 89.8260 | 89.8055 | 10 ₁₄₈ | 79.0893 | 79.0742 |
| 10 ₆₃ | 88.4046 | 88.3861 | 10 ₁₀₆ | 89.1546 | 89.1319 | 10 ₁₄₉ | 81.0500 | 81.0318 |
| 10 ₆₄ | 87.4878 | 87.4742 | 10 ₁₀₇ | 89.7525 | 89.7356 | 10 ₁₅₀ | 80.1392 | 80.1219 |
| 10 ₆₅ | 88.3918 | 88.3725 | 10 ₁₀₈ | 88.5137 | 88.4932 | 10 ₁₅₁ | 81.8414 | 81.8207 |
| 10 ₆₆ | 89.0275 | 89.0047 | 10 ₁₀₉ | 91.1966 | 91.1789 | 10 ₁₅₂ | 79.1715 | 79.1556 |
| 10 ₆₇ | 88.4741 | 88.4534 | 10 ₁₁₀ | 89.6275 | 89.6114 | 10 ₁₅₃ | 80.4764 | 80.4648 |
| 10 ₆₈ | 88.1199 | 88.1013 | 10 ₁₁₁ | 89.6677 | 89.6438 | 10 ₁₅₄ | 81.5405 | 81.5218 |
| 10 ₆₉ | 89.0983 | 89.0778 | 10 ₁₁₂ | 89.5744 | 89.5529 | 10 ₁₅₅ | 78.0648 | 78.0503 |
| 10 ₇₀ | 89.2068 | 89.1846 | 10 ₁₁₃ | 90.2239 | 90.2141 | 10 ₁₅₆ | 79.5639 | 79.5443 |
| 10 ₇₁ | 89.0853 | 89.0699 | 10 ₁₁₄ | 89.3062 | 89.2856 | 10 ₁₅₇ | 81.4731 | 81.4568 |
| 10 ₇₂ | 89.1974 | 89.1779 | 10 ₁₁₅ | 90.4340 | 90.4176 | 10 ₁₅₈ | 81.6398 | 81.6220 |
| 10 ₇₃ | 89.5332 | 89.5130 | 10 ₁₁₆ | 90.2703 | 90.2583 | 10 ₁₅₉ | 79.8863 | 79.8692 |
| 10 ₇₄ | 88.1285 | 88.1077 | 10 ₁₁₇ | 89.5335 | 89.5245 | 10 ₁₆₀ | 78.1529 | 78.1472 |
| 10 ₇₅ | 88.9725 | 88.9524 | 10 ₁₁₈ | 89.5261 | 89.5094 | 10 ₁₆₁ | 74.5460 | 74.5302 |
| 10 ₇₆ | 88.3673 | 88.3479 | 10 ₁₁₉ | 90.1394 | 90.1226 | 10 ₁₆₂ | 81.0033 | 80.9838 |
| 10 ₇₇ | 88.5689 | 88.5471 | 10 ₁₂₀ | 90.1862 | 90.1674 | 10 ₁₆₃ | 82.6629 | 82.6548 |
| 10 ₇₈ | 88.5548 | 88.5322 | 10 ₁₂₁ | 89.9375 | 89.9240 | 10 ₁₆₄ | 82.1862 | 82.1698 |
| 10 ₇₉ | 88.9647 | 88.9488 | 10 ₁₂₂ | 89.8258 | 89.8094 | 10 ₁₆₅ | 82.8211 | 82.8040 |
| 10 ₈₀ | 89.1669 | 89.1556 | 10 ₁₂₃ | 92.3646 | 92.3565 | | | |

TABLE 6. Part 1 of Knot and Link Types sorted by Ropelength

| Link | Link | Link | Link | Link | Link | Link | Link |
|------------|------------|------------|------------|------------|------------|------------|------------|
| 2_1^2 | 8_1^2 | 9_{48}^2 | 9_3 | 9_{15}^2 | 9_{18}^2 | 10_{21} | 10_{23} |
| 3_1^3 | 8_{10}^3 | 8_{10}^2 | 10_{143} | 9_{31}^2 | 9_{25}^2 | 10_{12} | 10_{100} |
| 4_1^2 | 9_{46} | 8_{14}^2 | 9_4 | 9_{21}^2 | 9_{24}^2 | 10_{10} | 10_{25} |
| 4_1 | 9_{50}^2 | 8_8^2 | 10_{129} | 9_{36}^2 | 9_{38} | 10_{22} | 10_{102} |
| 5_1 | 9_{61}^2 | 8_{14} | 9_1^2 | 9_{14}^2 | 10_{151} | 10_7 | 10_{103} |
| 5_2 | 9_{42} | 8_{12}^2 | 10_{134} | 9_{15} | 9_{39} | 10_{47} | 10_{53} |
| 5_1^2 | 9_{47}^2 | 9_{55}^2 | 9_5 | 9_{19} | 9_{34}^2 | 10_{48} | 10_{94} |
| 6_3^3 | 9_{51}^2 | 9_{46}^2 | 9_4^2 | 9_{26} | 9_{39}^2 | 10_{50} | 10_{44} |
| 6_1^2 | 8_1 | 10_{140} | 10_{130} | 9_6^3 | 9_{37}^2 | 10_{15} | 10_{99} |
| 7_2^2 | 9_{54}^2 | 8_{15} | 10_{148} | 9_{24} | 9_{12}^2 | 10_{16} | 10_{13} |
| 6_2^2 | 8_2^2 | 9_{49} | 10_{152} | 9_8^2 | 9_{40}^2 | 10_{64} | 10_{90} |
| 6_1 | 9_{45}^2 | 8_5^2 | 10_{147} | 10_{162} | 9_{11}^3 | 10_{28} | 10_{91} |
| 6_2 | 10_{124} | 8_{12} | 9_{35} | 9_{27}^2 | 9_{11}^2 | 10_{62} | 10_{58} |
| 7_8^2 | 8_3 | 9_{48} | 9_{13}^2 | 10_{149} | 9_7^3 | 10_{19} | 10_{79} |
| 6_1^3 | 8_2 | 9_{45} | 9_{19}^2 | 9_{22} | 9_{26}^2 | 10_{54} | 10_{75} |
| 6_3 | 8_4 | 9_{17}^3 | 9_2^2 | 9_{22}^2 | 9_{29}^2 | 10_{85} | 10_{56} |
| 6_2^3 | 9_{43} | 8_{13}^2 | 10_{156} | 9_{21} | 9_{33}^2 | 10_{36} | 10_{66} |
| 6_3^2 | 9_{44} | 9_{58}^2 | 9_6 | 9_8^3 | 10_{164} | 10_{52} | 10_{41} |
| 8_7^3 | 8_5 | 9_{15}^3 | 10_{137} | 9_{25} | 9_{34} | 10_{35} | 10_{71} |
| 8_{19} | 9_{44}^2 | 8_7^2 | 9_5^2 | 9_7^2 | 9_{30}^2 | 10_{68} | 10_{69} |
| 7_1 | 9_{57}^2 | 9_{14}^3 | 9_7 | 9_1^3 | 9_3^3 | 10_{74} | 10_{87} |
| 8_{20} | 9_{13}^3 | 8_{17} | 10_{146} | 9_{28} | 9_{10}^3 | 10_{37} | 10_{106} |
| 7_2 | 8_7 | 10_{161} | 9_{10} | 9_{37} | 9_{12}^3 | 10_{31} | 10_{80} |
| 7_3 | 8_1^3 | 8_6^3 | 10_{159} | 9_{27} | 9_4^3 | 10_{49} | 10_{72} |
| 7_1^2 | 9_{59}^2 | 10_{132} | 9_9 | 9_{29} | 10_{138} | 10_{33} | 10_{70} |
| 7_4 | 9_{18}^3 | 8_3^3 | 9_3^2 | 10_{135} | 10_{163} | 10_{51} | 10_{59} |
| 8_{15}^2 | 8_9 | 9_{47} | 9_{14} | 9_{35}^2 | 9_{38}^2 | 10_{14} | 10_{29} |
| 8_8^3 | 8_6 | 9_{21}^3 | 9_8 | 10_{131} | 9_{33} | 10_{38} | 10_{40} |
| 7_2^2 | 8_4^2 | 8_{18} | 10_{127} | 9_{23} | 10_{165} | 10_{39} | 10_{114} |
| 7_4^2 | 9_{19}^3 | 10_{125} | 9_{12} | 9_{28}^2 | 9_{41}^2 | 10_{76} | 10_{60} |
| 7_5 | 8_3^2 | 8_4^3 | 9_6^2 | 9_{41} | 9_{42}^2 | 10_{30} | 10_{43} |
| 7_3^2 | 8_8 | 9_{16}^3 | 9_{16} | 9_{16}^2 | 10_1 | 10_{55} | 10_{97} |
| 8_{21} | 8_{13} | 8_1^4 | 9_{20}^2 | 9_{32}^2 | 10_3 | 10_{65} | 10_{89} |
| 7_7 | 9_{52}^2 | 9_1 | 9_{11} | 10_{144} | 10_2 | 10_{93} | 10_{45} |
| 7_6 | 9_{56}^2 | 10_{142} | 10_{150} | 10_{157} | 10_4 | 10_{63} | 10_{118} |
| 7_1^3 | 10_{139} | 10_{145} | 9_{36} | 9_{30} | 10_8 | 10_{24} | 10_{73} |
| 9_{49}^2 | 8_{11} | 9_{20}^3 | 9_{20} | 9_{32} | 10_{46} | 10_{18} | 10_{117} |
| 7_5^2 | 8_2^3 | 10_{128} | 9_{23}^2 | 10_{154} | 10_{61} | 10_{26} | 10_{96} |
| 9_{43}^2 | 8_{10} | 10_{141} | 9_5^3 | 9_9^3 | 10_5 | 10_{67} | 10_{83} |
| 8_3^4 | 8_{11}^2 | 10_{133} | 9_{13} | 9_{18} | 10_6 | 10_{108} | 10_{88} |
| 7_6^2 | 8_6^2 | 10_{126} | 9_9^2 | 9_1^4 | 10_9 | 10_{78} | 10_{112} |
| 8_9^3 | 8_9^2 | 10_{136} | 9_{17}^2 | 10_{158} | 10_{20} | 10_{77} | 10_{57} |
| 8_{16}^2 | 8_5^3 | 10_{155} | 9_{10}^2 | 9_{40} | 10_{11} | 10_{32} | 10_{92} |
| 8_2^4 | 8_{16} | 9_2 | 9_{17} | 9_{31} | 10_{34} | 10_{82} | 10_{110} |
| 9_{53}^2 | 9_{60}^2 | 10_{160} | 10_{153} | 9_2^3 | 10_{17} | 10_{86} | 10_{111} |
| 8_1^2 | 9_{48}^2 | 9_3 | 9_{15}^2 | 9_{18}^2 | 10_{21} | 10_{23} | 10_{84} |

TABLE 7. Part 2 of Knot and Link Types sorted by Ropelength

| Link | Link | Link | Link | Link | Link | Link |
|------------|------------|------------|------------|------------|------------|------------|
| 10_{84} | 10_{107} | 10_{27} | 10_{95} | 10_{120} | 10_{115} | 10_{123} |
| 10_{98} | 10_{105} | 10_{42} | 10_{81} | 10_{113} | 10_{109} | |
| 10_{101} | 10_{122} | 10_{121} | 10_{119} | 10_{116} | 10_{104} | |
| 10_{107} | 10_{27} | 10_{95} | 10_{120} | 10_{115} | 10_{123} | |

TABLE 8. Part 1 of Residuals of Tight Knots and Links by Knot Type

| Link | Residual | Link | Residual | Link | Residual | Link | Residual |
|---------|-----------------|------------|-------------|------------|-----------------|------------|-------------|
| 2_1^2 | $2.45124e - 05$ | 8_2 | 0.000982684 | 8_8^3 | 0.00100655 | 9_{38} | 0.000978978 |
| 3_1 | 0.00621792 | 8_3 | 0.00100028 | 8_9^3 | 0.000980533 | 9_{39} | 0.000999482 |
| 4_1 | 0.000996335 | 8_4 | 0.00100103 | 8_{10}^3 | 0.0208108 | 9_{40} | 0.000999343 |
| 4_1^2 | 0.000999549 | 8_5 | 0.00100033 | 8_1^4 | 0.00100006 | 9_{41} | 0.00899161 |
| 5_1 | 0.00981995 | 8_6 | 0.000999848 | 8_2^4 | 0.000999682 | 9_{42} | 0.000999996 |
| 5_2 | 0.00994775 | 8_7 | 0.00101551 | 8_3^4 | 0.780186 | 9_{43} | 0.00898749 |
| 5_1^2 | 0.00998078 | 8_8 | 0.000981272 | 9_1 | 0.00802077 | 9_{44} | 0.000999789 |
| 6_1 | 0.000999592 | 8_9 | 0.000999932 | 9_2 | 0.00997484 | 9_{45} | 0.0099754 |
| 6_2 | 0.00897204 | 8_{10} | 0.000978418 | 9_3 | 0.00998254 | 9_{46} | 0.00099973 |
| 6_3 | 0.000979541 | 8_{11} | 0.000979921 | 9_4 | $8.64059e - 05$ | 9_{47} | 0.000998991 |
| 6_1^2 | 0.000999952 | 8_{12} | 0.00998976 | 9_5 | 0.00999417 | 9_{48} | 0.00998933 |
| 6_2^2 | 0.000999833 | 8_{13} | 0.000993117 | 9_6 | 0.000980197 | 9_{49} | 0.00099957 |
| 6_3^2 | 0.00999004 | 8_{14} | 0.000981486 | 9_7 | 0.000979897 | 9_1^2 | 0.00107787 |
| 6_1^3 | 0.00998537 | 8_{15} | 0.0099948 | 9_8 | 0.00101007 | 9_2^2 | 0.00100115 |
| 6_2^3 | 0.000705159 | 8_{16} | 0.000981316 | 9_9 | 0.000999938 | 9_3^2 | 0.00100055 |
| 6_3^3 | 0.00627026 | 8_{17} | 0.00999085 | 9_{10} | 0.00113523 | 9_4^2 | 0.00099991 |
| 7_1 | 0.00105833 | 8_{18} | 0.000900015 | 9_{11} | 0.000981742 | 9_5^2 | 0.00100118 |
| 7_2 | 0.00998149 | 8_{19} | 0.000998339 | 9_{12} | 0.000979842 | 9_6^2 | 0.00126944 |
| 7_3 | 0.00999358 | 8_{20} | 0.00099998 | 9_{13} | 0.00999582 | 9_7^2 | 0.00104121 |
| 7_4 | 0.00100877 | 8_{21} | 0.000999988 | 9_{14} | 0.000984327 | 9_8^2 | 0.00100133 |
| 7_5 | 0.000999532 | 8_1^2 | 0.00100142 | 9_{15} | 0.000979831 | 9_9^2 | 0.000999724 |
| 7_6 | 0.000979869 | 8_2^2 | 0.000979836 | 9_{16} | 0.000999818 | 9_{10}^2 | 0.00140283 |
| 7_7 | 0.00100393 | 8_3^2 | 0.000999961 | 9_{17} | 0.00100032 | 9_{11}^2 | 0.000999221 |
| 7_1^2 | 0.000999487 | 8_4^2 | 0.00216462 | 9_{18} | 0.00992217 | 9_{12}^2 | 0.00100137 |
| 7_2^2 | 0.00101952 | 8_5^2 | 0.00999516 | 9_{19} | 0.000981217 | 9_{13}^2 | 0.00100112 |
| 7_3^2 | 0.000999871 | 8_6^2 | 0.00100295 | 9_{20} | 0.00100005 | 9_{14}^2 | 0.000999788 |
| 7_4^2 | 0.00099954 | 8_7^2 | 0.000999802 | 9_{21} | 0.00100001 | 9_{15}^2 | 0.000999236 |
| 7_5^2 | 0.000999894 | 8_8^2 | 0.000999762 | 9_{22} | 0.00098846 | 9_{16}^2 | 0.00605 |
| 7_6^2 | 0.00100556 | 8_9^2 | 0.000979774 | 9_{23} | 0.000998846 | 9_{17}^2 | 0.00899775 |
| 7_7^2 | 0.00320787 | 8_{10}^2 | 0.000999858 | 9_{24} | 0.000979562 | 9_{18}^2 | 0.000999648 |
| 7_8^2 | 0.0018494 | 8_{11}^2 | 0.00997927 | 9_{25} | 0.000999907 | 9_{19}^2 | 0.00100405 |
| 7_1^3 | 0.000999748 | 8_{12}^2 | 0.000999968 | 9_{26} | 0.000977105 | 9_{20}^2 | 0.000999853 |
| 8_1 | 0.00898769 | 8_{13}^2 | 0.0010008 | 9_{27} | 0.00100048 | 9_{21}^2 | 0.00898977 |
| 8_2 | 0.000982684 | 8_{14}^2 | 0.00101123 | 9_{28} | 0.00999324 | 9_{22}^2 | 0.00943088 |
| | | 8_{15}^2 | 0.00099994 | 9_{29} | 0.00996501 | 9_{23}^2 | 0.000998181 |
| | | 8_{16}^2 | 0.000997563 | 9_{30} | 0.000979844 | 9_{24}^2 | 0.000999946 |
| | | 8_1^3 | 0.00100589 | 9_{31} | 0.000979942 | 9_{25}^2 | 0.0009999 |
| | | 8_2^3 | 0.000999904 | 9_{32} | 0.000979062 | 9_{26}^2 | 0.00100243 |
| | | 8_3^3 | 0.00100014 | 9_{33} | 0.000997746 | 9_{27}^2 | 0.00099997 |
| | | 8_4^3 | 0.00999606 | 9_{34} | 0.00100114 | 9_{28}^2 | 0.000998883 |
| | | 8_5^3 | 0.000995844 | 9_{35} | 0.000999697 | 9_{29}^2 | 0.00100157 |
| | | 8_6^3 | 0.00099824 | 9_{36} | 0.000981383 | 9_{30}^2 | 0.00099989 |
| | | 8_7^3 | 0.00119532 | 9_{37} | 0.000978472 | 9_{31}^2 | 0.000999523 |
| | | 8_8^3 | 0.00100655 | 9_{38} | 0.00999228 | 9_{32}^2 | 0.00100012 |
| | | | | | 0.000978978 | 9_{33}^2 | 0.000999711 |

TABLE 9. Part 2 of Residuals of Tight Knots and Links by Knot Type

| Link | Residual | Link | Residual | Link | Residual | Link | Residual |
|------------|-------------|------------|-------------|-----------|-------------|------------|-------------|
| 9_{33}^2 | 0.000999711 | 9_{16}^3 | 0.000999575 | 10_{37} | 0.000999835 | 10_{82} | 0.000978946 |
| 9_{34}^2 | 0.00100169 | 9_{17}^3 | 0.247874 | 10_{38} | 0.000979821 | 10_{83} | 0.00999433 |
| 9_{35}^2 | 0.000999778 | 9_{18}^3 | 0.000999841 | 10_{39} | 0.000986038 | 10_{84} | 0.0099812 |
| 9_{36}^2 | 0.00100172 | 9_{19}^3 | 0.00101035 | 10_{40} | 0.00100863 | 10_{85} | 0.000981325 |
| 9_{37}^2 | 0.000999058 | 9_{20}^3 | 0.00100002 | 10_{41} | 0.00999693 | 10_{86} | 0.000978499 |
| 9_{38}^2 | 0.000999748 | 9_{21}^3 | 0.00100039 | 10_{42} | 0.000999751 | 10_{87} | 0.000979621 |
| 9_{39}^2 | 0.000999888 | | | 10_{43} | 0.000980157 | 10_{88} | 0.000979845 |
| 9_{40}^2 | 0.000999835 | 9_1^4 | 0.000979958 | 10_{44} | 0.00322255 | 10_{89} | 0.0010019 |
| 9_{41}^2 | 0.00100037 | | | 10_{45} | 0.000982692 | 10_{90} | 0.000980234 |
| 9_{42}^2 | 0.000998679 | 10_1 | 0.00101691 | 10_{46} | 0.00997656 | 10_{91} | 0.000977397 |
| 9_{43}^2 | 0.00100109 | 10_2 | 0.00100023 | 10_{47} | 0.000980999 | 10_{92} | 0.00100005 |
| 9_{44}^2 | 0.00100838 | 10_3 | 0.000991435 | 10_{48} | 0.00999602 | 10_{93} | 0.000979652 |
| 9_{45}^2 | 0.00997492 | 10_4 | 0.00100846 | 10_{49} | 0.000998073 | 10_{94} | 0.00097991 |
| 9_{46}^2 | 0.00100042 | 10_5 | 0.00100194 | 10_{50} | 0.000981787 | 10_{95} | 0.000979668 |
| 9_{47}^2 | 0.00999831 | 10_6 | 0.000979506 | 10_{51} | 0.00098231 | 10_{96} | 0.00018365 |
| 9_{48}^2 | 0.000999984 | 10_7 | 0.0097283 | 10_{52} | 0.000999419 | 10_{97} | 0.000999872 |
| 9_{49}^2 | 0.000999984 | 10_8 | 0.000980356 | 10_{53} | 0.00101025 | 10_{98} | 0.00999481 |
| 9_{50}^2 | 0.000999226 | 10_9 | 0.000979784 | 10_{54} | 0.00999263 | 10_{99} | 0.0099926 |
| 9_{51}^2 | 0.000999443 | 10_{10} | 0.00999688 | 10_{55} | 0.00998728 | 10_{100} | 0.00101003 |
| 9_{52}^2 | 0.000999958 | 10_{11} | 0.00760935 | 10_{56} | 0.00999185 | 10_{101} | 0.00999705 |
| 9_{53}^2 | 0.00996962 | 10_{12} | 0.000991292 | 10_{57} | 0.000999798 | 10_{102} | 0.000979674 |
| 9_{54}^2 | 0.000999703 | 10_{13} | 0.000999947 | 10_{58} | 0.000999966 | 10_{103} | 0.00999479 |
| 9_{55}^2 | 0.00100064 | 10_{14} | 0.0010261 | 10_{59} | 0.00995441 | 10_{104} | 0.00999683 |
| 9_{56}^2 | 0.000979788 | 10_{15} | 0.000979185 | 10_{60} | 0.000980266 | 10_{105} | 0.000979902 |
| 9_{57}^2 | 0.00255237 | 10_{16} | 0.000985699 | 10_{61} | 0.0241498 | 10_{106} | 0.000979055 |
| 9_{58}^2 | 0.000999155 | 10_{17} | 0.00998848 | 10_{62} | 0.00105699 | 10_{107} | 0.000980096 |
| 9_{59}^2 | 0.00108631 | 10_{18} | 0.000979621 | 10_{63} | 0.00998227 | 10_{108} | 0.00127554 |
| 9_{60}^2 | 0.000999312 | 10_{19} | 0.00098045 | 10_{64} | 0.00997603 | 10_{109} | 0.000979798 |
| 9_{61}^2 | 0.00100091 | 10_{20} | 0.000979959 | 10_{65} | 0.00135295 | 10_{110} | 0.000979638 |
| | | 10_{21} | 0.000999057 | 10_{66} | 0.000999872 | 10_{111} | 0.000979851 |
| 9_1^3 | 0.000999763 | 10_{22} | 0.000991413 | 10_{67} | 0.000979823 | 10_{112} | 0.00104599 |
| 9_2^3 | 0.000999746 | 10_{23} | 0.00999682 | 10_{68} | 0.00100695 | 10_{113} | 0.00999934 |
| 9_3^3 | 0.00100525 | 10_{24} | 0.00166886 | 10_{69} | 0.000999786 | 10_{114} | 0.00100087 |
| 9_4^3 | 0.000999641 | 10_{25} | 0.000994731 | 10_{70} | 0.000980057 | 10_{115} | 0.000978725 |
| 9_5^3 | 0.00100042 | 10_{26} | 0.00098015 | 10_{71} | 0.00999226 | 10_{116} | 0.00998661 |
| 9_6^3 | 0.000999746 | 10_{27} | 0.000999869 | 10_{72} | 0.000999942 | 10_{117} | 0.00998396 |
| 9_7^3 | 0.000999935 | 10_{28} | 0.00996703 | 10_{73} | 0.00998888 | 10_{118} | 0.00099987 |
| 9_8^3 | 0.000999751 | 10_{29} | 0.00116525 | 10_{74} | 0.000978382 | 10_{119} | 0.000999834 |
| 9_9^3 | 0.000996684 | 10_{30} | 0.000999376 | 10_{75} | 0.000981812 | 10_{120} | 0.00100037 |
| 9_{10}^3 | 0.00099985 | 10_{31} | 0.000979897 | 10_{76} | 0.000980892 | 10_{121} | 0.00099989 |
| 9_{11}^3 | 0.0010755 | 10_{32} | 0.000979993 | 10_{77} | 0.00999768 | 10_{122} | 0.000999203 |
| 9_{12}^3 | 0.00100439 | 10_{33} | 0.000979857 | 10_{78} | 0.000981017 | 10_{123} | 0.0016528 |
| 9_{13}^3 | 0.00980919 | 10_{34} | 0.00098555 | 10_{79} | 0.0010001 | 10_{124} | 0.00100133 |
| 9_{14}^3 | 0.00900147 | 10_{35} | 0.000982115 | 10_{80} | 0.000979926 | 10_{125} | 0.00998345 |
| 9_{15}^3 | 0.00112426 | 10_{36} | 0.000979692 | 10_{81} | 0.000981576 | 10_{126} | 0.00999723 |
| 9_{16}^3 | 0.000999575 | 10_{37} | 0.000999835 | 10_{82} | 0.000978946 | 10_{127} | 0.00998882 |

TABLE 10. Part 3 of Residuals of Tight Knots and Links by Knot Type

| Link | Residual | Link | Residual | Link | Residual | Link | Residual |
|-------------------|-------------|-------------------|-------------|-------------------|-------------|-------------------|-------------|
| 10 ₁₂₇ | 0.00998882 | 10 ₁₃₇ | 0.000979856 | 10 ₁₄₇ | 0.000999813 | 10 ₁₅₇ | 0.000979535 |
| 10 ₁₂₈ | 0.000988223 | 10 ₁₃₈ | 0.00899453 | 10 ₁₄₈ | 0.000981385 | 10 ₁₅₈ | 0.000980822 |
| 10 ₁₂₉ | 0.00902523 | 10 ₁₃₉ | 0.000979731 | 10 ₁₄₉ | 0.00100026 | 10 ₁₅₉ | 0.000979791 |
| 10 ₁₃₀ | 0.000999987 | 10 ₁₄₀ | 0.0099924 | 10 ₁₅₀ | 0.000979903 | 10 ₁₆₀ | 0.00998455 |
| 10 ₁₃₁ | 0.00959976 | 10 ₁₄₁ | 0.00100144 | 10 ₁₅₁ | 0.000979813 | 10 ₁₆₁ | 0.00899311 |
| 10 ₁₃₂ | 0.000980876 | 10 ₁₄₂ | 0.000980204 | 10 ₁₅₂ | 0.00999625 | 10 ₁₆₂ | 0.000985909 |
| 10 ₁₃₃ | 0.000980018 | 10 ₁₄₃ | 0.00993363 | 10 ₁₅₃ | 0.0091785 | 10 ₁₆₃ | 0.00899697 |
| 10 ₁₃₄ | 0.00999485 | 10 ₁₄₄ | 0.00995796 | 10 ₁₅₄ | 0.00115132 | 10 ₁₆₄ | 0.000979519 |
| 10 ₁₃₅ | 0.00100006 | 10 ₁₄₅ | 0.00102699 | 10 ₁₅₅ | 0.00998753 | 10 ₁₆₅ | 0.000979783 |
| 10 ₁₃₆ | 0.00999149 | 10 ₁₄₆ | 0.00998505 | 10 ₁₅₆ | 0.0009799 | | |
| 10 ₁₃₇ | 0.000979856 | 10 ₁₄₇ | 0.000999813 | 10 ₁₅₇ | 0.000979535 | | |